



HAL
open science

3D structural and thermal modelling of Mesozoic petroleum systems in the Po Valley Basin, northern Italy

Claudio Turrini, Barbara Bosica, Paul Ryan, Peter Shiner, Olivier Lacombe, Francois Roure

► **To cite this version:**

Claudio Turrini, Barbara Bosica, Paul Ryan, Peter Shiner, Olivier Lacombe, et al.. 3D structural and thermal modelling of Mesozoic petroleum systems in the Po Valley Basin, northern Italy. *Petroleum Geoscience*, 2018, 24 (2), pp.172. 10.1144/petgeo2017-031 . hal-01630270

HAL Id: hal-01630270

<https://hal.sorbonne-universite.fr/hal-01630270>

Submitted on 7 Nov 2017

HAL is a multi-disciplinary open access archive for the deposit and dissemination of scientific research documents, whether they are published or not. The documents may come from teaching and research institutions in France or abroad, or from public or private research centers.

L'archive ouverte pluridisciplinaire **HAL**, est destinée au dépôt et à la diffusion de documents scientifiques de niveau recherche, publiés ou non, émanant des établissements d'enseignement et de recherche français ou étrangers, des laboratoires publics ou privés.

3D structural and thermal modelling of Mesozoic petroleum systems in the Po Valley basin, northern Italy

Claudio Turrini (1), Barbara Bosica (2), Paul Ryan (3), Peter Shiner (2), Olivier Lacombe (4), and François Roure (5, 6)

1. *CTGeolConsulting, 78100, St.Germain-en-Laye, France (clturri@wanadoo.fr)*
2. *Petroceltic Italia, Via E.Q: Visconti 20, Roma 00193, Italy*
3. *Petroceltic International plc, 3 Grand Canal Plaza, Grand Canal Street Upper, Dublin 4, Ireland*
4. *Sorbonne Universités, UPMC Univ Paris 06, CNRS, Institut des Sciences de la Terre de Paris (iSTeP), 4 place Jussieu 75005 Paris, France*
5. *IFP-EN, Rueil-Malmaison, France*
6. *Tectonic Group, Utrecht University, the Netherlands*

Abstract

1D and 3D basin modelling was performed to investigate the Mesozoic carbonate petroleum systems of the Po Valley basin (northern Italy), through integration of a recent 3D structural model of the study area with the distribution of potential Triassic source rocks, rock property, and heat flow models.

Results from standard 1D maturity models show significant over-prediction of the thermal maturity of deep Triassic carbonates in the western Po Valley, unless the effect of the substantial overpressure observed in these sequences is incorporated into the model. In order to further test this observation, two thermal scenarios were applied to the Po Valley 3D geovolume: one based on the actual geological heat flow and a second model based on a reduced heat flow as a proxy for the delaying effect of overpressure on hydrocarbon maturation. The predictions of these two models were then compared with the observed hydrocarbon distribution in the western Po Valley.

Both thermal scenarios are broadly consistent with the observed hydrocarbon distribution at the scale of the basin, but in detail, the overpressure model provides a better match between the predicted charge available from the kitchen areas post-critical moment and

33 observed volumes of hydrocarbons initially in place within the traps, as well as with the
34 observed and predicted hydrocarbon phases, as measured by the gas/oil ratio (GOR) of the
35 fluids. Overpressure probably significantly delayed hydrocarbon maturation in the western
36 domain of the basin, confirming results from previous studies.

37 Beyond regional implications, and despite its relative simplicity and inherent
38 uncertainties, the adopted approach demonstrates the potential of a consistent 3D integration of
39 the thermo-structural history of sedimentary basins to constrain the geometry and structural
40 evolution of hydrocarbon-bearing traps as well as the generation and migration of hydrocarbons
41 into these traps.

42

43 **Key-words:** 3D thermo-structural models, thermal maturity, Po Valley tectonics and
44 hydrocarbons, overpressure, Northern Italy

45

46

47 The Po Valley (Northern Italy) (Fig.1a) is the foreland-foredeep basin of the Southern
48 Alps and the Northern Apennines thrust-belts and forms one of the best known hydrocarbon
49 provinces in continental Europe (Errico et al., 1980; Pieri & Groppi, 1981; Pieri, 1984; Cassano
50 et al., 1986; Riva et al., 1986; Bongiorni, 1987; Mattavelli & Novelli, 1987; Nardon et al., 1991;
51 Mattavelli & Margarucci, 1992; Mattavelli et al., 1993; Lindquist, 1999; Casero, 2004; Bertello
52 et al., 2010). The basin stratigraphy consists of a thick (4000-10000m) carbonate-clastic
53 sedimentary section with both oil and gas having been produced from different levels across
54 the basin. In this framework, the deep Mesozoic carbonates represent the preferential target for
55 oil exploration whereas the overlying clastic intervals of Miocene, Pliocene and Pleistocene age
56 are principally drilled for shallow gas accumulations.

57 Despite the long history of exploration-production activity and the progression of data
58 and knowledge acquisition from both academia and industry, the thermal history of the Po
59 Valley region has been poorly documented in the public literature (Wygrala, 1988; Chiaramonte
60 & Novelli, 1986), which has focused primarily on the temperature evolution of similar units
61 cropping out in the adjacent Southern Alps fold-and-thrust units (Bersezio & Bellantani, 1997;
62 Greber et al., 1997; Calabrò et al., 2003; Fantoni & Scotti, 2003; Scotti, 2005; Carminati et al.,
63 2010).

64 In an attempt at gathering all available structural and stratigraphic datasets into a
65 comprehensive view, Turrini et al. (2014) have produced a 3D structural model of the entire Po

66 Valley basin. This model provides a spatially consistent structural geo-volume of the Po Valley,
67 which allows better constraint of the influence of structural inheritance on the kinematic
68 evolution of this foreland-foredeep system (Turrini et al., 2016) and better integration of the
69 seismotectonics (Turrini et al, 2015).

70 As a further step toward a better understanding of the Po Valley hydrocarbon generation
71 potential, we construct a regional, hydrocarbon-maturity-oriented structural and thermal model
72 of the buried Mesozoic succession of the Po Valley. This approach relies upon the combination
73 of our 3D structural model with a 1D and 3D thermal modelling of the entire Po Valley basin,
74 with focus on the proven (Bertello et al., 2010) deep Mesozoic carbonates petroleum system.
75 In particular, we aim to model and review the timing of trap formation across the Po Valley
76 foreland-foredeep domain relative to the progressive maturation and generation history of the
77 known Triassic source rocks. The possible impact of overpressure on hydrocarbon maturation
78 is further addressed through thermal modelling considering both the actual geologic heat flow
79 and a reduced heat flow aimed at approximating the delaying effects of overpressure on
80 hydrocarbon maturation and generation. Beyond regional implications, this study demonstrates
81 the utility and applicability of an integrated 3D basin modelling approach to better constrain
82 the geometry and structural evolution of hydrocarbon-bearing traps in sedimentary basins as
83 well as the generation and migration of hydrocarbons into these traps. Notably, the study
84 confirms that the delaying effect of overpressure can be an important factor to be taken into
85 account in predictions of hydrocarbon maturation and generation.

86

87 **The Po Valley basin**

88

89 *Regional geologic setting*

90

91 The geological architecture of the Po Valley basin has been discussed in many recent
92 papers covering the different structural-stratigraphic aspects of the region (e.g., Turrini et al.,
93 2014, 2015, 2016 and references therein).

94 The Po Valley basin is a complex basin system that developed as a nearly simultaneous
95 pro/retro foreland-foredeep of the diachronous and opposite verging Northern Apennines and
96 Southern Alps mountain belts. During Mesozoic and Cenozoic times, the Po Valley domain
97 was affected by repeated extensional and compressional events (Fig.1b). These tectonic events
98 essentially relate to the long-lasting geodynamic effects produced by Tethyan rifting and

99 drifting, and subsequent oceanic subduction and collision of the Adria and Eurasian plates
100 (Dewey et al., 1973; Castellarin, 2001; Carminati & Doglioni, 2012; Pfiffner, 2014 and
101 references therein). Indeed, the present-day structural pattern is primarily the result of Mesozoic
102 extension and Cenozoic compression (Pieri & Groppi, 1981; Bongiorni, 1987; Cassano et al.,
103 1986; Castellarin et al., 1985; Fantoni et al., 2004, Ravaglia et al., 2006; Fantoni & Franciosi,
104 2010; Turrini et al., 2014 and references therein). From Paleogene to present times, the
105 amplification and propagation of the Northern Apennines and Southern Alps belts controlled
106 the differential flexure of the Po Valley-Adria lithosphere, the associated tilting and bulging of
107 the foreland domain, the rapid sedimentation of thick foredeep-type deposits and their
108 successive involvement within the developing tectonic wedges (e.g., Carminati & Doglioni,
109 2012 and references therein).

110 Mainly Miocene-to-Pleistocene thrusting is dominant across the shallow Tertiary
111 sediments whereas a large part of the basin substratum (Mesozoic and basement) shows
112 evidence of the pre-compressional tectonic grain, with autochthonous highs and lows of
113 extension-related origin, partially reactivated by compression. Interference between the
114 extension-related structures (approximately north-south trending) and the compression-related
115 ones (generically west-east trending) is a primary characteristic within the basin (e.g., Turrini
116 et al., 2016) which, given the earthquake distribution, is considered a more active tectonic
117 province as one moves from west to east (Michetti et al., 2013; Vannoli et al., 2014; Turrini et
118 al., 2015 and references therein).

119 The main stratigraphic units across the basin consist of Triassic platform carbonates,
120 Jurassic to Cretaceous platform and basinal carbonates, overlain by Tertiary clastics (Fig.1c)
121 (Jadoul, 1986; Cati et al., 1987; Jadoul et al., 1992; De Zanche et al., 2000; Ghielmi et al., 2012;
122 Masetti et al., 2012; Pfiffner, 2014). This sedimentary package appears to overlie some Permian
123 sediments and their Hercynian metamorphic basement (Fig.1c). The latter has been drilled by
124 a few wells within the basin and locally crops out in the hinterland of the Southern Alps and
125 the Northern Apennines (Cassano et al., 1986; Ponton, 2010; Pfiffner, 2014).

126

127 *Exploration history*

128

129 Exploration for hydrocarbons in the Po Valley started in the first half of the 20th century
130 (Pieri, 1984). Soon after the second world war, the investigations progressively covered the
131 north-east of the basin while the use of electric well logs and cores, the development of updated

132 micro-palaeontological techniques and, especially, the acquisition of analogue seismic data
133 enabled the recognition and understanding of deeper targets. This resulted in the drilling of the
134 Caviaga 1 well, (1944; 1404 m TD bsl – below sea level), the first gas field discovered by Agip
135 within the Po Valley and the largest in Western Europe at that time. Between 1945 and 1982,
136 the newly acquired digital seismic allowed the very deep horizons to be imaged, also favouring
137 the development of new hypotheses concerning deep lithologies and their associated rock
138 properties. In the 1980s, new methodologies led to the detailed analysis of the seismo-
139 stratigraphy and the associated structural setting and style of the basin. The integration of well
140 correlations with seismic interpretation resulted in the construction of the regional base-
141 Pliocene structural map by Pieri & Groppi (1981). From 1973 to 1984, hydrocarbon exploration
142 of the Mesozoic carbonates developed through investigation of both overthrust structures
143 developed during Alpine orogenesis and drilling of Mesozoic structural highs formed by
144 Triassic-Liassic rifting (Bongiorni, 1987; Bertello et al., 2010). Both types of targets proved to
145 be successful and led to the discovery of four major hydrocarbon fields, namely the Malossa
146 (gas condensate), Cavone, Gaggiano and Villafortuna (oil) fields. The latter is one of the largest
147 oil fields in continental Europe and has produced 226 million barrels (MMbbl) of light oil to
148 date from a record depth of 6000 m bsl. Today the Po Valley stands as an under-explored region
149 ready for the next exploration phase, with the help of exploitation of updated technologies
150 integrated with increased knowledge of the basin geology.

151

152 *Hydrocarbon systems and hydrocarbon distribution*

153

154 Various petroleum systems have been identified and defined on the basis of drilling,
155 outcrop geology and systematic analysis of the associated oil and gas types (Riva et al., 1986;
156 Bongiorni, 1987; Mattavelli et al., 1993; Wygrala, 1988; Lindquist, 1999; Bello & Fantoni,
157 2002; Franciosi & Vignolo, 2002; Casero, 2004; Bertello et al., 2010).

158 The Triassic-Liassic petroleum systems have produced gas, condensate and light oil
159 from deep Mesozoic carbonates (Fig.1c). The reservoir consists of dolomitized carbonate
160 platform units of middle Triassic–Early Jurassic age, charged by middle to Late Triassic
161 carbonate source rocks deposited in intra-platform lagoons and basins. Traps are mostly
162 provided by Mesozoic extensional structures locally inverted during the Cenozoic compression.
163 The Cretaceous-Jurassic pelagic carbonates provide the regional seal. The Villafortuna-Treccate
164 Field (discovered in 1984; light oil; 226 MMbbl of 43° API oil and 93 billion of cubic feet (bcf)
165 of gas produced to date), represents the largest oil accumulation associated with this play (Bello

166 & Fantoni 2002; Bertello et al., 2010). Second-order oil fields in terms of both size and
167 production are the Malossa field (discovered in 1973; gas and condensate; approximately 27
168 MMbbl and 150 bcf gas produced) (Errico et al., 1980; Pieri & Groppi, 1981; Mattavelli &
169 Margarucci, 1992), the Cavone field (discovered in 1974; 23°API oil; 94.5 MMbbl
170 hydrocarbons initially in place HCIIP) (Nardon et al., 1991) and the Gaggiano field (discovered
171 in 1982; 36°API oil; 20-30 MMbbl estimated reserves) (Bongiorni, 1987; Rigo 1991; Fantoni
172 et al., 2004).

173 The Oligo-Miocene petroleum system (Fig.1c) produces thermogenic gas with
174 secondary quantities of oil from the foredeep successions which are detached and thrust over
175 the carbonates and belong to the Northern Apennine belt (Mattavelli & Novelli, 1987,
176 Mattavelli et al., 1993; Bertello et al., 2010). The system is composed of thick turbidite
177 sequences that supply both the reservoir, source and seal elements and the traps are usually
178 structural, with the Cortemaggiore and Casteggio fields as typical examples of producing fields
179 related to this petroleum system.

180 The Plio-Pleistocene petroleum system contains large volumes of biogenic gas (Fig.1c),
181 notably at the buried external fronts of the Apennine thrust belt (Mattavelli & Novelli, 1987,
182 Mattavelli et al., 1993; Lindquist, 1999; Casero, 2004; Bertello et al., 2010). The system
183 consists of sand-rich turbidites in which thick-bedded sand lobes and thin-bedded, fine-grained
184 basin plain/lobe fringe deposits are the main reservoir facies associations (Ghielmi et al. 2012).
185 Interbedded clays are both the source-rock and the effective topseal. Traps are most commonly
186 structural, yet stratigraphic traps also occur, mainly related to the onlap of turbidite reservoirs
187 onto the flanks of thrust propagation folds or against the foreland ramp. The Settala field (1977)
188 is a remarkable example of a mixed structural–stratigraphic trap in the Plio-Pleistocene play
189 (Bertello et al., 2010).

190 The 3D basin model discussed in this paper specifically addresses the burial and
191 temperature history of the thermogenic Mesozoic petroleum system. The Plio-Pleistocene and
192 Oligo-Miocene systems are not discussed hereinafter.

193

194 **Methods, input data and modelling assumptions: building and calibrating the thermo-** 195 **structural model of the Po Valley at the Mesozoic carbonate level**

196

197 Data used for the 3D structural model come from public literature and the archives of
198 the Italian Ministry of Energy (<http://unmig.sviluppoeconomico.gov.it>, namely the ViDEPI
199 project). These data include geological cross-sections, well composite logs as well as

200 geophysical and geological maps. No seismic data have been used during the model building
201 process because: a) they are poorly distributed across the study area, b) they are generally low-
202 quality images, c) their integration into the model would have required a questionable time-
203 depth conversion, uncertain due to simplifications in the estimated velocity distribution related
204 to the widely varying lithologies in the study area. A full description of the whole dataset, and
205 its distribution across the basin, is provided in Turrini et al. (2014, 2015, 2016). The structural
206 model was built using Midland Valley's MOVE software (<http://www.mve.com/>) while
207 progressive refinement of the 3D grids and fault pattern was carried out using IHS's Kingdom
208 interpretation package ([https://www.ih.com/products/kingdom-seismic-geological-
209 interpretation-software.html](https://www.ih.com/products/kingdom-seismic-geological-interpretation-software.html)).

210 The resulting Po Valley 3D structural model (Turrini et al., 2014, 2015) consists of 66
211 faults and 5 layer grids, namely: the Moho discontinuity, the basement, the near top Triassic,
212 the top Mesozoic Carbonates, and the base Pliocene. At all levels within the model, the regional-
213 scale architecture indicates the presence of two crustal domains, a western and an eastern
214 domain separated by the Giudicarie Lineament, a NE-SW oriented feature dissecting the basin
215 (Fig.2). Shallow structures are formed by folds and thrusts in the Tertiary clastic succession.
216 Deep structures relate to faulting of the Mesozoic carbonates and their basement, with local
217 inversion of pre-compressional basins and thin-skinned tectonic imbrication (Fig.3). The area
218 of interest for the present study is strictly limited to the Northern Apennines and Southern Alps
219 foreland domain in order to exclude major tectonic over-thickening across the Mesozoic
220 structures that would have biased the thermal modelling results (see white stippled line in
221 Fig.2).

222 Data used to populate the thermal model (back-stripping and thermal parameters,
223 temperature and heat flow data, palaeo-water depths, total organic carbon – TOC -, hydrogen
224 index – HI - values, etc.) are taken from published literature and publicly available well data
225 (Riva et al., 1986; Mattavelli & Novelli, 1987; Wygrala, 1988; Fantoni & Scotti, 2003, ViDEPI
226 Project) as well as a limited amount of proprietary data. Modelling was carried out using
227 Zetaware Inc.'s Genesis & Trinity 3D software packages (<http://www.zetaware.com/>) and
228 proprietary spreadsheets.

229 The basin modelling workflow for this study consisted of three phases, described in
230 detail in subsequent sections of this paper. The workflow is summarized in Table 1.

231

232 *Model structural geometries at the Mesozoic carbonate level*

233

234 The Villafortuna field, the Gaggiano field and the Lacchiarella structure, and the
235 Malossa field are the most significant structures at the Mesozoic carbonate level which are
236 considered in the thermal modelling. Despite being located outside the area covered by the
237 thermal model, the Cavone structure is also described to complement the overall picture. Such
238 structures a) illustrate the common deformation features affecting the Mesozoic carbonates in
239 the Po Valley foreland, b) are related to the major tectonic events experienced in the region
240 (Mesozoic extension and Cenozoic compression) and c) illustrate the main trap types for the
241 deep Mesozoic oil play within the basin.

242

243 **The Villafortuna field:** The Villafortuna field (Figs. 2 and 3a, 4) corresponds to a major
244 compressional structure that involves the Mesozoic section and the underlying basement (Pieri
245 & Groppi, 1981; Cassano et al., 1986; Bello and Fantoni, 2002; Turrini et al., 2014, 2016). The
246 structure is weakly displaced towards the NW and wedges into the overlying Tertiary
247 sediments, which, in turn, are thrust to the SE along the Romentino front (RF in Fig.4a, c, d).
248 The base Pliocene unconformity separates the deformed Oligo-Miocene succession from the
249 undeformed Plio-Pleistocene deposits. The field structure consists of a dome-type anticline,
250 regionally plunging towards the SW and the NE (Fig.2 and 4a). Faults are SE and NW-dipping
251 thrusts that cut down to the basement while controlling the gentle, final pop-up geometry below
252 the Tertiary package (Fig.3 and 4c-d). Displacement is essentially towards the NW with an
253 average throw of some 3 km at top carbonate level. In perspective and map view, the faults
254 show an en-echelon pattern (Fig.4b). The presence of a complete late and middle Triassic
255 reservoir-source section is reported within the field while a few hundred meters of Jurassic-
256 early Cretaceous, basinal carbonates provide the likely topseal (Casero, 2004 and references
257 therein; Bertello et al., 2010). According to the final 3D model, the trap area of the field is
258 approximately 100 km² and likely compartmentalized by Triassic-Jurassic normal faults
259 (Casero, 2004 and references therein). These, given the lack of public information, could not
260 be represented inside the structural model. The geometrical relationship between Tertiary
261 sediments and the Mesozoic-basement assemblage within the Villafortuna tectonic wedge
262 suggests that the age of the trap is mainly late Miocene (Turrini et al., 2016) with displacement
263 of a pre-compressional Triassic high (Fig. 4c).

264

The Gaggiano field and the Lacchiarella structure: The Gaggiano-Lacchiarella structure (Fig.5) is a crustal-scale tectonic feature which cuts across the entire Po Valley basin and extends towards the Southern Alps to the north and the Northern Apennines to the south (see Gaggiano location in Fig.2). This feature has a complex history: it initiated as a north-south striking, east-dipping extensional fault system in the Liassic, underwent initial inversion in the Oligocene and was weakly reactivated during the Miocene (Fantoni et al., 2004; Turrini et al., 2016). Liassic extension resulted in significant footwall erosion over the crest of the Gaggiano footwall high and in the deposition of an expanded section of deep-water Jurassic and Cretaceous carbonates in the subsiding Lacchiarella hangingwall basin. Oligocene inversion resulted in approximately no net extension at top Triassic level across the feature. Inversion and vertical expulsion of the thickened Jurassic-Cretaceous deep-water carbonate sediments, originally deposited in the Lachiarella hanging wall basin resulted in a regional north-south striking anticline immediately to the east of, and above, the trace of the extensional Liassic fault system (Fig.5). The structural framework derives from the overprinting of Mesozoic extensional and Tertiary compressional tectonics, as revealed by 2D sections through the model volume (see Fig.5c-e). Major faults in the region are east-dipping whereas the associated secondary faults are west-dipping, with the two fault sets bounding the Gaggiano high and the Lacchiarella basin. The Gaggiano field (Fig.3a and 5) is located on the west-dipping footwall crest of the north-south Triassic-Liassic extensional fault system (Cassano et al., 1986; Bongiorno, 1987; Fantoni et al., 2004; Turrini et al., 2014, 2016). Within the field, the Mesozoic section is extremely thinned by erosion associated with syn-extensional footwall uplift. basement is encountered by wells at the exceptionally shallow depths of approximately 5 km bsl (Fig. 5c-e). Based on the 3D model reconstruction, the top reservoir at Gaggiano lies just below the top Mesozoic surface, at an average depth of 4.5 km bsl, giving a closure of approximately 30 km² and defining a relatively limited four-way-dip closure at the crest of the regional footwall (Bongiorno, 1987). This trap was formed by Liassic extension and underwent minor rotation during the Cenozoic, along with the deposition of Oligo-Miocene foredeep sediments. The top-seal is provided by intra-platform basinal carbonates (Meride formation), which also form the source rock for the field (Bongiorno, 1987; Bertello et al., 2010). Wells drilled on the Lacchiarella inversion structure (Lacchiarella-2 – 1978 - and San Genesio - 1994) have encountered significantly increased thicknesses of Jurassic and Cretaceous basinal limestones, confirming the overall tectono-stratigraphic model, but have failed to encounter significant hydrocarbons at the Triassic objective levels.

299 **The Malossa field** : The Malossa field (Fig.3a - 6) is located in the western sector of the Milano
300 tectonic arc (see Fig.2). The field is one of a number of structures which deform the Po Valley
301 Mesozoic foreland and have been buried beneath the Tertiary foredeep wedges to the south of
302 the Southern Alps belt (Errico et al., 1980; Pieri & Groppi, 1981; Cassano et al., 1986;
303 Mattavelli & Margarucci, 1992; Fantoni & Franciosi, 2010; Turrini et al., 2014). The reservoir
304 of the field is provided by fractured late Triassic platform carbonates while the overlying
305 Jurassic-Cretaceous basinal carbonates constitute the seal, along with some further reservoir
306 sections. The source rock has not been proven within the field area. However, analysis of the
307 oil (Mattavelli & Novelli, 1987; Mattavelli & Margarucci, 1992; Bertello et al., 2010) suggests
308 a late Triassic source rock (Argilliti di Riva di Solto), a lithology which crops out extensively
309 in the Southern Alps, to the north of the Malossa region (Fantoni & Scotti, 2003). Stratigraphy
310 from the well information indicates the presence of a Triassic-Liassic high. The trap is provided
311 by a NW-SE oriented, faulted anticline, plunging towards both the NW and the SE. The
312 associated major thrust is NE dipping and it displaces the structure towards the SW. Minor
313 faults are reported to intersect the fold crest, creating structural compartments within the field
314 (Mattavelli & Margarucci, 1992). From the structural model, the average depth to the top
315 Mesozoic structural crest is 5 km bsl, while the field area is approximately 15 km² (Fig.6a). The
316 final age of trap formation is mainly late Miocene with some minor reactivation during the Plio-
317 Pleistocene (Turrini et al., 2016).

318 The 3D model (Fig.6) shows that the Malossa structure was formed by folding and
319 thrusting of the Mesozoic carbonates and the related basement. Sections through the model
320 volume (Fig.6c-e) confirm that inversion of the Triassic-Liassic extensional basins controls the
321 overall structural style in the region (Cassano et al., 1986; Ravaglia et al., 2006; Fantoni &
322 Franciosi, 2010; Masetti et al., 2012) with both reactivation of Mesozoic extensional faults and
323 creation of new faults, which locally cut through the pre-existing highs. The Chiari and
324 Belvedere structures, to the NE of the Malossa field are significant, and together with the
325 Lacchiarella structure (see section 4.1.2, Fig. 5), are the main evidence of the basin inversion
326 that took place in the western Po Valley domain (cf. Figures 12 & 13 in Turrini et al., 2016).

327 Key-characteristics of these two structures, as compared to Malossa are as follows: (a)
328 the structures are inverted Liassic half-grabens and the thick (5 km) Mesozoic carbonates are
329 vertically extruded by Miocene inversion (the Malossa structure is essentially a pre-existing

330 Triassic-Liassic high deformed by Cenozoic thrusting); (b) the Mesozoic faults are reactivated
331 (if the map shown by Mattavelli & Margarucci, (1992) is considered correct, it is possible to
332 argue that pre-compressional faults – not represented in the 3D model - are passively displaced
333 by new thrusts in the Malossa structure); (c) some tectonic over-thickening of the Jurassic
334 sediments can be interpreted from the public composite log (the Malossa well data does not
335 appear to show any tectonic repetition); (d) the basement is involved in the structuration (as at
336 Malossa); (e) the age of the present structural geometries is essentially late Miocene with some
337 minor contribution from Pliocene tectonics (as at Malossa).

338

339 **The Cavone field:** The Cavone field (Fig.3b-7) is situated on the lateral ramp of a major
340 tectonic arc (i.e. the Ferrara arc) at the buried front of the eastern Northern Apennines (see
341 Fig.2) (Pieri & Groppi, 1981; Cassano et al., 1986; Nardon et al., 1991; Turrini et al., 2014,
342 2016). The structure is a thrust-related fold where Mesozoic and Tertiary sediments are
343 intensely faulted and fractured (Cassano et al., 1986; Nardon et al., 1991; Carannante et al.,
344 2014). The age of the trap is essentially Plio-Pleistocene although Miocene tectonics might have
345 contributed to the early stage development of the field (Castellarin et al., 1985; Nardon et al.,
346 1991; Ghielmi et al., 2012; Turrini et al., 2016). The 3D structural model shows the imbrication
347 of the Mesozoic units and the clear asymmetry of the associated thrust-related fold (see Fig.7):
348 as such, faults inside the tectonic stack are mainly SSE dipping and the derived faulted anticline
349 is NNW verging (Fig.7c). The observed vertical throw that separates the Cavone hanging-wall
350 and foot-wall units (i.e. the Po Valley foreland) is around 1.5 km on average. The structural
351 geometry described suggests a major detachment surface at the base of the Triassic sediments
352 (arrow in Fig.7c & d) and makes any involvement of the basement particularly unlikely
353 (Cassano et al., 1986; Nardon et al., 1991) unless short-cutting and slicing of the footwall of
354 the foreland unit has occurred (Carannante et al., 2014). The depth to the Cavone culmination
355 from the available public data is approximately 3 km bsl, to near top Mesozoic and and 4 km
356 bsl to top Triassic respectively. According to the reconstructed geometry, the field area would
357 be in the order of 30 km² (Fig.7a, c, d).

358

359 *Defining source rock distribution and building Gross Depositional Environment (GDE) maps*
360 *in the Mesozoic carbonates*

361 Middle and Late Triassic intervals (Fig. 8a) are the major source rocks for the deep
362 Mesozoic petroleum system of the Po Valley (Mattavelli & Novelli, 1987; Mattavelli et al.,
363 1993; Zappaterra, 1994; Lindquist, 1999; Katz et al., 2000; Casero, 2004; Bertello et al., 2010).
364 A description of the spatial distribution of these source intervals (Fig. 8b-c) and the assignation
365 of the related main parameters describing hydrocarbon generation potential (net source
366 thickness, TOC, HI etc.) (Table 1) are, as a consequence, key inputs for the basin modelling.
367 The present section describes how the source model was constrained within the 3D basin model.

368 The definition of the source rock depositional setting and basin geometry across the Po
369 Valley is a rather difficult task. Indeed: a) the tectonic history of the basin is complex and
370 polyphased; b) only a few deep wells have drilled through the Triassic source intervals; c)
371 mapping the lateral extent of the source rocks is not easy, given the lack of a clear seismic
372 expression in the basins where the source rocks were deposited. Source rock distribution in the
373 model is consequently described by the construction of Gross Depositional Environment maps
374 (GDE maps) produced for key intervals.

375

376 Two loosely defined tectonically-controlled megasequences can be identified: a) a
377 mainly middle Triassic (Anisian to late Carnian) megasequence, associated with extensional-
378 transtensional tectonics and local volcanism driven by plate scale wrench movements or aborted
379 rifting; and b) a mainly late Triassic (late Carnian to early Liassic) megasequence, associated
380 with Tethyan rifting. The middle Triassic megasequence (Fig. 8a) commences with the tectonic
381 segmentation of the widespread epeiric carbonate-evaporitic platform system that dominated in
382 the early Triassic. From the late Anisian onwards, intra-platform basins developed and euxinic
383 conditions occurred periodically. This regional setting resulted in the deposition of organic-rich
384 basinal carbonates over the entire Po Valley realm: the Meride limestone, the Besano and Gorno
385 formations were deposited in the Western Po Valley whereas the Livinallongo formation, the
386 bituminous events in the Predil Limestone and the Rio del Lago formation were deposited in
387 the Eastern Po Valley. From the early Carnian onwards, subsidence slowed and platform
388 carbonates prograded across the basins ending this first phase of deposition of organic-rich
389 facies. The gross depositional environment map in Figure 8b shows the interpreted spatial
390 distribution of potential source rock basins for this megasequence; in the western Po Valley,
391 such basins are interpreted to have an approximately north-south orientation, whilst in the
392 eastern Po Valley, the basins are interpreted as oriented north-east to south-west (Franciosi &
393 Vignolo, 2002). In the western Po valley, two potential source basins are identified: the Anisian
394 to Ladinian Meride-Besano basin and the Carnian Gorno basin, situated to the west and east of

395 Milan, respectively. The source potential of the former is confirmed by geochemical correlation
396 with the oils from the Villafortuna-Treccate and Gaggiano fields (Bello & Fantoni, 2002). The
397 source rock potential of the Gorno basin is more speculative: the enrichment of organic matter
398 is reported from outcrops (Stefani & Burchill, 1990, Assereto et al, 1977, Wygrala, 1988) within
399 sediments deposited in shallow anoxic lagoons developed within a mixed clastic-carbonate
400 depositional system (Gnaccolini & Jadoul, 1990). Nevertheless, little direct evidence exists for
401 hydrocarbons having been generated in the subsurface from that formation. Indeed, extension
402 of this facies southwards, into the subsurface of the Po Valley is exclusively based on the
403 occurrence of an analogous facies in one of the wells within the Malossa field. In the Central
404 Po Valley, along the buried Ferrara arc (i.e. the buried, external front of the Northern
405 Apennines), the presence of a Mid Triassic source basin is inferred from the Cavone field oil-
406 source correlation: this indicates a middle Triassic oil-prone carbonate source rock similar to
407 the Meride Formation of the western Po Valley (Mattavelli & Novelli, 1987; Nardon et al.,
408 1991). In the eastern Po Valley and Adriatic foreland, the distribution of potential source basins
409 is taken from Franciosi & Vignolo (2002) with two offshore middle Triassic basins identified,
410 the Ada and Amelia basins, as constrained by 3D seismic. However, the presence of source
411 rock facies remains speculative. Onshore, organic-enriched middle Triassic (Anisian-Carnian)
412 basinal marls and wackestones up to several tens of metres thick are known within the thick
413 basinal successions of the Livinallongo, Predil, Rio del Lago and Durrenstein Formations of
414 the south eastern Alps (Brack & Rieber, 1993; Fantoni & Scotti 2003; Keim et al 2006). Similar
415 facies are encountered in the subsurface of the Po Valley at the Villaverla-1 well: these facies
416 can be interpreted to lie within one of several north-east to south-west oriented basins, of similar
417 dimensions to those mapped offshore on 3D seismic data (proto-Belluno trough, Masetti et al.
418 2012).

419 Extensional tectonics during the middle-late Norian in the Central Southern Alps and in
420 the Carnian Pre-Alps resulted in the progressive segmentation of the widespread Dolomia
421 Principale carbonate platform formed during late Carnian and early Norian quiescence.
422 Extension developed approximately north-south oriented, intra-platform basins up to several
423 tens of kilometres wide (Jadoul et al., 1992) which expanded as rifting progressed in the Liassic.
424 Drowning of large sectors of the platform led to fully open marine deep-water conditions which
425 were associated with the Tethyan-Ligurian Ocean. Eventually, restricted anoxic conditions
426 developed during the Late Triassic. This resulted in the preservation of high levels of organic
427 material within the basinal limestone facies, for example in the Argilliti di Riva di Solto, Zu,
428 and Aralalta formations in the Central Po Valley, and the Dolomia di Forni of the Eastern Po

429 Valley. The GDE map in Figure 8c shows the interpreted spatial distribution of these potential
430 source basins: the main basin in the western Po valley is the Riva di Solto basin of mid to late
431 Norian age. This basin developed in the subsiding hanging wall of the major late Triassic-
432 Liassic Gaggiano-Lacchiarella extensional fault system (Fantoni & Franciosi, 2010). Thinner
433 sequences of organic-rich sediments were also deposited in a mid to outer ramp setting, in the
434 overlying Rhaetian carbonate ramp represented by the Zu Formation (Stefani & Burchill 1990,
435 Galli et al 2007). The source potential of these successions is well documented both from
436 outcrop (Jadoul et al., 1992) and geochemical typing of the oils from the Malossa field data
437 (Mattavelli & Novelli, 1987). In the eastern Po valley, the upper megasequence commences
438 with a widespread late Carnian transgression, resulting in deposition of the organic-rich
439 dolomites of the Monticello Formation, in an inner ramp setting. An organic-rich facies, about
440 60m thick, ascribed to this interval is reported in the offshore Adriatic foreland at the Amanda-
441 1bis well (Carulli et al 1997). As transgression continued into the Norian, differentiation
442 occurred in areas dominated by the widespread Dolomia Principale Platform, passing laterally
443 into narrow (km to a few tens of km) anoxic basins. An example is the area of the future Belluno
444 Trough where the organic rich Dolomia di Forni was deposited (Carulli et al 1997), locally
445 attaining thicknesses of 850m. Within the Dolomia Principale, anoxic intra-platform lagoons
446 developed locally and these are reported (Carulli et al 1997) onshore, in the eastern Southern
447 Alps (over 100m of laminated dolomites and “scisti bituminosi” at Rio Resartico) and in the
448 Adriatic offshore (the Amanda-1bis well).

449 The GDE maps (Fig.8b-8c) were used to define the lateral source rock distribution
450 within the 3D basin model. Source parameters were then assigned to each polygon. The net
451 thickness of source intervals is poorly constrained: the gross thickness of the source-bearing
452 interval may locally reach 1 km inside the major depocentres (Pieri, 2001) whilst Fantoni et al.
453 (2002) define 400m of gross thickness for the Meride-Besano source interval in the
454 Villafortuna-Treccate field. On this basis, net source thickness has been assigned with reference
455 to the interpreted GDE, with a) long-lived anoxic basins assigned a net source thickness of 50m,
456 b) episodically anoxic basins assigned 25m, and c) intra-platform/ ramp anoxic lagoons
457 assigned 12.5m.

458 In general, potential source rocks are carbonate-argillaceous sediments with TOC
459 varying from a maximum of 40% in the Besano Shales to a minimum of 0.10% within the
460 Meride Limestone, with an average of ~ 4% (Novelli et al., 1987, Fantoni et al., 2002, Katz et
461 al, 2000). Kerogen types are dominantly of marine origin, with a secondary component of
462 terrestrial material. For all source rocks within the model, those kerogen types have been

463 parameterized as 90% Type-A kerogen and 10% Type-F kerogen, using default kinetic
464 parameters as defined by Pepper & Corvi (1995a-b) and as shown in Table 2. The only
465 exceptions are the potential source rocks of the Gorno Formation which are described as
466 dominantly consisting of reworked terrestrial material (Stefani & Burchill, 1990) and have
467 consequently been parameterized as 10% Type-A kerogen and 90% Type-F kerogen.

468 The petroleum potentials derived from these source parameters are reported in Table 2.
469 They appear to be consistent with those reported in the literature: Fantoni et al (2002) suggest
470 a formation average petroleum potential for the Meride-Besano interval at Villafortuna-Treccate
471 of 21 kg of hydrocarbons per ton (HC/ton) of rock, whilst Bello & Fantoni (2002) indicate a
472 source potential index of 4t of hydrocarbons per square meter (HC/m²)(or 30 million barrels
473 per square km - MMbbl/km²) for the mid Triassic petroleum system of the western Po Valley
474 and of 3t HC/m² (or 22 MMbbl/km²) for the Late Triassic petroleum system.

475

476 *Model rock physical properties*

477 The rock properties used as input for modelling include the following: 1) chrono-litho-
478 stratigraphy; 2) surface porosities; 3) compaction coefficients; 4) bulk densities; 5) radiogenic
479 heat generation parameters for each lithology; 6) thermal conductivities and their temperature
480 dependencies. These parameters were mainly derived from exploration wells or adjacent
481 outcrop analogues (Berra & Carminati, 2010, Pasquale et al 2011, Pasquale et al, 2012) (Table
482 3).

483 The chrono-litho-stratigraphic section used in the 1D modelling was built by assigning
484 the percentages of end member lithologies present for each stratigraphic unit described (Fig
485 9a). Back-stripping and thermal properties were defined based on lithology. For mixed
486 lithologies, properties are derived from the end member lithologies combined with the relative
487 percentage of each using the appropriate mixing model: simple volumetric weighting is used to
488 calculate surface porosity, compaction coefficient, density, volumetric heat capacity and
489 radioactive heat generation, whilst thermal conductivities are calculated using a geometric
490 mixing law (Pasquale et al. 2011). Temperature dependency of thermal conductivity is
491 incorporated into the model using an approximation to the Sekiguchi Correction (Sekiguchi,
492 1984). A summary of the properties assigned for each end member lithology is given in Table
493 3.

494 *Model pressure in the Mesozoic carbonates*

495

496 The Mesozoic carbonates of the western Po valley are characterized by high
497 overpressures and these represent a significant challenge to deep exploration (Pietro et al., 1979;
498 Vaghi et al., 1980). Early workers argued that formation pressure exerted a significant control
499 on hydrocarbon maturation in the area, by illustrating a correlation of the possible overpressures
500 with the difference between observed and theoretically calculated measures of maturity
501 (Chiaramonte & Novelli, 1986). While using a global dataset that included data points from the
502 western Po Valley, subsequent investigations highlighted the relationship between vitrinite
503 reflectance and formation overpressure (Carr, 1999). This work resulted in a quantitative model
504 based on modifying the Easy%Ro algorithm of Sweeney & Burnham (1990), which is based
505 on the temperature history of a sample, to include an overpressure term. Following the emphasis
506 placed by previous workers in the area on overpressure as a delaying factor on thermal maturity,
507 one of the objectives of the present study was to investigate this effect and, should its
508 importance be confirmed, incorporate it into the 3D basin modelling.

509 Novelli et al (1987) briefly reviewed the overpressure distribution in the western portion
510 of the study area. This distribution is characterized by a normally pressured shallow clastic
511 aquifer of Pliocene age and a deep, overpressured carbonate aquifer of Triassic age. This latter
512 corresponds to the units that host the Triassic petroleum systems discussed in this paper. The
513 two aquifers are separated by an aquitard consisting of fine-grained clastic rocks of Miocene to
514 Paleogene age and fine-grained basinal carbonates of Paleogene to Jurassic age. This aquitard
515 is characterized by a strong pressure ramp connecting the normally pressured shallow aquifer
516 to the overpressured deep carbonate aquifer. These authors interpret overpressures as due to
517 high sedimentation rates associated with foredeep sedimentation from the Oligocene onwards.
518 Hydraulic isolation of the deep carbonate aquifer occurred during middle to late Miocene times
519 due to Alpine thrusting, resulting in creation of the deep carbonate pressure cell, in the western
520 Po Valley. Eventually, rapid burial during the Plio-Pleistocene produced the present distribution
521 of overpressure within both the deep carbonate aquifer and the mixed clastic-carbonate
522 aquitard.

523 In this study, the data and models presented by Novelli et al. (1987) were extended in
524 two ways: a) by creating 1D pore pressure models for both the aquitard and the deep carbonate
525 aquifer (for key wells), as an input to modelling the thermal maturity of organic matter; b) by
526 reviewing the distribution of overpressures within the deep carbonate aquifer against the
527 structure maps from the 3D model, while developing an understanding of the spatial and
528 temporal distribution of these overpressures.

529 The 1D pore pressure models for individual wells were built in two steps: firstly a
530 constant overpressure was estimated for the deep carbonate aquifer, based either on pressure
531 data from the well in question or from data presented by Novelli et al (1987) (their Fig. 7);
532 secondly available pressure data (primarily mud-weight data, but with occasional well test or
533 MDT data) in the aquitard were modelled using the Mann & Mackenzie (1990) approach; in
534 this process, the Plio-Pleistocene sedimentation rate was one key input whilst lithology within
535 the aquitard and top overpressure were other key inputs (Mann & Mackenzie, 1990). An
536 example of such a model is shown in Fig. 9b for the Belvedere well.

537 The 3D structural model clearly indicates that the overpressures are confined to a
538 regional scale anticline developed at the Top Triassic level in the western Po valley (thick red
539 line in Fig. 2), and that this anticline was in place by the end of the Miocene, although it
540 probably formed sometime in the Paleogene (Turrini et al., 2016; see trap formation map in
541 Figure 15). This anticline is isolated from the normally pressured carbonates of the eastern Po
542 valley (e.g. the Malpaga-1 well; Novelli et al., 1987), across the Chiari syncline (Fig.2) which
543 takes the Triassic sediments to a depth of 8-8.5 km bsl.

544

545 *Model water depths and heat flow*

546

547 Palaeo-water depths were inferred from a) the depositional facies locally defined at the
548 different well locations and b) the GDE maps for key intervals (Fig.8b-c). These depths broadly
549 correlate with those considered by Winterer & Bosellini (1981) for the Mesozoic carbonates
550 and by Di Giulio et al. (2013) and Ghielmi et al. (2012) for the Cenozoic. Finally, sediment-
551 surface interface and palaeo-temperatures are derived by combining palaeo-water surface
552 temperatures based on the relative latitude of the Po Valley through time with a discrete water
553 depth-temperature relationship such as that proposed by Defant (1961).

554 The heat flow model (Fig. 10) has been defined following a comparative review of
555 published data, primarily from the Southern Alps (Mattavelli & Novelli, 1987; Greber et al.,
556 1997; Fantoni & Scotti, 2003; Zattin et al., 2006; Scotti & Fantoni, 2008; Carminati et al., 2010;
557 Grobe et al., 2015). There is general consensus around two episodes of increased heat flow
558 during the Mesozoic: the first in the middle Triassic, caused by a first pulse of extensional
559 tectonic activity, which resulted in the development of the basins where the middle Triassic
560 source rocks were deposited; the second during the early Jurassic, associated with the full
561 development of Tethyan rifting. A late Cenozoic reduction in the heat flow trend is observed
562 due to high sedimentation rates and rapid burial in the foredeep, related to the advancing

563 Southern Alps and Northern Apennine fronts. This is consistent with the basin geodynamics
564 and associated tectono-stratigraphic evolution of the Po Valley region (see section 2.1). The
565 present day heat flow has been estimated on the regional map of Italy of Della Vedova et al.
566 (2001), with corrected well temperature data where available.

567

568 *Calibration of 1D thermal model and assumptions underlying overpressure modelling*

569

570 A number of well locations, with available temperature and/or maturity data, were
571 selected for 1D modelling to provide a reasonable geographic spread across the Po Valley
572 region. Maturity data are mainly collected from the literature (particularly Wygrala, 1988;
573 Chiaramonte & Novelli, 1986; Fantoni & Scotti, 2003) with the addition of some proprietary
574 data. Furthermore, some pseudo-wells were constructed to fill in the areas where well data
575 were sparse. The chrono- and litho-stratigraphy for each well were derived from the relevant
576 composite log, with physical properties (porosity, density, thermal conductivity) being assigned
577 based on lithology as described in section 3.3. Measured temperature data reported on the
578 composite log were corrected to in-situ temperature using the approach described by Pasquale
579 et al. (2012). In general, the available maturity data for the Mesozoic carbonates were limited
580 and of poor quality, frequently showing substantial scatter. Much of the data consists of
581 maximum Temperature (Tmax) values from Rock-Eval pyrolysis analysis. Those data were
582 converted to vitrinite reflectance (%Ro) equivalent values using the relationship of Jarvie et al.
583 (2001). The satisfactory nature of this relationship in the study area was confirmed at wells with
584 both Tmax and vitrinite reflectance data available.

585 As a first calibration step, the present-day temperature-depth relationship calculated
586 from the model was compared with the corrected temperature values derived from the
587 composite log. An example is the Belvedere-1 well (Fig. 9c). In general, the match between
588 model and observation was acceptable particularly over the targeted carbonate section. Once a
589 good match was obtained between temperature observations and predictions from the model,
590 maturity profiles were calculated for each well and pseudo-well. Additionally, for wells with
591 maturity data, the calculated profile was compared with observed data. As an example, Figure
592 9d clearly indicates that the maturity profile calculated by the Easy %Ro algorithm (which uses
593 only the temperature history of each data point, Burnham & Sweeney, 1989) for the Belvedere-
594 1 well, substantially over-predicts the observed thermal maturity: this is particularly true in the
595 Mesozoic carbonates. In contrast, algorithms that incorporate the overpressure history, in
596 addition to the temperature history, appear to produce a better fit to the observed data, with the

597 PresRo algorithm of Carr (1999) producing very similar results to the alternative T-P-Ro
598 algorithm of Zou & Peng (2001). It is noteworthy that Carr,1999, incorporates overpressure
599 effects into the Easy%Ro model by introducing a pressure based modification to the frequency
600 factor, whilst Zou & Peng, 2001, introduce an overpressure based modification to the activation
601 energies. For the purposes of this modelling exercise, it was assumed that pressures were
602 hydrostatic up to the end Miocene isolation of the deep carbonate aquifer in the western Po
603 valley. From the end of the Miocene onwards it was assumed that overpressures increased
604 linearly with time up to the present day values modelled for a particular interval. As for the
605 Belvedere 1, other wells included in the dataset showed similar results, with an improved fit to
606 observed maturity data from models incorporating overpressure and over-prediction of maturity
607 using Easy%Ro. Of particular note at the Belvedere-1 well is the way in which the results of
608 the overpressure algorithms converge with the Easy %Ro model below 7,500m tvdss (Fig.9d).
609 This is likely due to peak maturity deep within the carbonate section having been achieved
610 during the Liassic rift event, long before significant overpressure entered the system. Such an
611 early maturity was a consequence of the thick syn-rift section deposited at this location,
612 combined with elevated heat flows. Notwithstanding the relatively poor quality and scattered
613 nature of the maturity data, this analysis would appear to support the inference that overpressure
614 has delayed the thermal maturity of the Triassic source rocks in parts of the Po Valley as
615 suggested by Chiaramonte & Novelli (1986) and Carr (1999).

616 The Genesis and Trinity 3D modelling software from Zetaware, Inc. used in this study
617 does not incorporate algorithms that include the overpressure effect. The most appropriate
618 modelling strategy was therefore to approximate the overpressure effect in the software by
619 applying a reduced heat flow, given that overpressure appears to act to delay maturation (Carr,
620 1999). Figure 9d shows that the maturity profiles calculated for the Belvedere-1 well using the
621 overpressure algorithms are approximated by a temperature-only maturity model using a heat
622 flow that is 15m watts per square meter (W/m^2) lower than the currently observed heat flow at
623 this location. Hence, to replicate the overpressure history in the basin, the reduced heat flow
624 model was built to equal the geological heat flow up to the end of the Miocene. From that
625 moment, the heat flow was varied linearly to reach a present day value that is $15mW/m^2$ lower
626 than the observed present day heat flow. Similar results were obtained for other wells in the
627 dataset. This analysis was also repeated for a number of pseudo-well data points covering the
628 depth range of the Triassic source rocks within the model overpressure cell. This operation
629 confirms that a reduced heat flow model satisfactorily replicates the maturity trends generated
630 by the overpressure model.

631

632 **Modeling results**

633 *1D thermal model and hydrocarbon generation*

634

635 The results from 1D modelling for well and pseudo-well locations in the western,
636 central, east-central and eastern Po Valley are summarized in Figure 11. For the western and
637 central Po Valley, two sets of results are provided, one based on the actual geological heat flow
638 and one which considers the effect of overpressure through application of the reduced heat flow
639 model from end Miocene times. In the western Po Valley, west of Milan (Fig. 11a), the Triassic
640 source intervals reached maturity during the Miocene as a result of burial beneath the thick
641 Alpine foredeep sediments. These source rocks are currently in the late oil window. In contrast,
642 in the central Po Valley east of Milan (Fig. 11b), Triassic source rocks started generating
643 hydrocarbons during the Jurassic, with renewed generation in the Miocene, and are currently in
644 the late oil to gas windows. This generation process is probably due to the increased thickening
645 of syn-rift Liassic carbonates in the hanging wall of the Gaggiano-Lacchiarella fault system,
646 combined with high syn-rift heat flows. For both the western and central Po Valley well
647 locations, the reduced heat flow / overpressure model shows lower maturity, all through Plio-
648 Pleistocene. In the western Po Valley, this equates to the difference between middle oil maturity
649 ($\%Ro \approx 0.8$) and wet gas maturity ($\%Ro \approx 1.3$).

650 Over most of the eastern Po Valley, middle Triassic source rocks attained early maturity
651 during the Jurassic (Fig. 11c) due to thick carbonate deposition and high heat flows, with only
652 minor increases in maturity to present day as a result of lower heat flow and/or a low
653 sedimentary depositional rate. During the same time interval, Late Triassic source rocks
654 remained immature to very early mature (Fig. 11c). Figure 11d shows the 1D model for part of
655 the Trento Platform in the eastern Po Valley where sedimentation rates remained particularly
656 low. In this location only limited generation potential is envisaged, with the early oil window
657 being reached by the middle Triassic source rocks in the late Miocene to Recent, whilst late
658 Triassic source rocks are essentially immature at the present day.

659

660 *3D thermal model and hydrocarbon generation*

661

662 Results from 1D modelling (see above) and GDE maps have been integrated with the
663 3D structural model to create a 3D thermal model of the entire Po Valley foreland basin. Using

664 the 1D well models as anchor points, two thermal histories were created and calibrated to best
665 represent the thermal histories of the Middle and Late Triassic source intervals, one based on
666 the actual geological heat flow model and one based on the reduced heat flow to replicate the
667 effect of overpressure. In particular, the reduced heat flow associated with the overpressure
668 model is confined to the area of the regional scale anticline at Top Triassic level that contains
669 the overpressure cell, as shown in Fig. 2. Outside this area, the two heat flow models are equal.

670 The progressive change in transformation ratio through time across the Po Valley for
671 the middle and late Triassic source intervals from the Mesozoic to the end Miocene is illustrated
672 in Figure 12. For middle Triassic source rocks early oil maturity is attained during the Jurassic
673 to the east of the Gaggiano Lacchiarella fault system and in most of the eastern Po Valley whilst
674 to the west maturity remains low (Fig 12a). This clearly fits the 1D modelling scenarios and
675 confirms the results presented by Novelli et al., 1987.

676 The maturity pattern is attributed to high syn-rift heat flows associated with Liassic
677 rifting, combined with the deposition of a) thick sequences of basinal limestones in the
678 hangingwall of the Gaggiano Lacchiarella fault system, b) thick shallow marine carbonate
679 deposits in the area of the Trento Platform (Fig. 2) and c) thinner basinal sequences to the west
680 (footwall) of the Gaggiano Lacchiarella tectonic trend. Through the Cretaceous only small
681 increases in maturity are observed due to low sedimentation rates in a deep-water, basinal
682 setting. During this period, heat flows returned to typical passive margin setting levels (Fig.
683 12b) (Fantoni & Scotti, 2003). Remarkably in Jurassic and Cretaceous times, the Late Triassic
684 source rocks remain immature, except in the vicinity of locally thick carbonate deposits,
685 particularly in the central and north-western Po Valley (Fig.12d-e).

686 During the early Tertiary and up to the end of the Miocene, the enhanced clastic influx
687 from the Southern Alpine and Northern Apennines thrust belts increased burial of both Triassic
688 source intervals with further increases in maturity. Locally, where sedimentation rates were
689 highest, such as in portions of the Southern Alpine foredeep, this resulted in the completion of
690 the kerogen transformation process (Fig 12c-f). Notwithstanding this, the Liassic structural
691 grain continued to exert an influence on maturity patterns with much of the Gaggiano footwall
692 and Trento Platform constantly exhibiting low maturities.

693 In middle to late Miocene times, the deep carbonate aquifer in the western Po Valley
694 became isolated and the Triassic source intervals started to experience overpressure. Figure 13
695 compares the present-day transformation ratio distribution for the actual geological heat flow
696 and reduced heat flow /overpressure models. The high Plio-Pleistocene sedimentation rate
697 resulted in increased maturity throughout the Po valley, however, as expected, within the

698 western Po Valley overpressure cell, the increase in maturity is substantially less for the
699 overpressure model than for the geological heat flow model (compare Figs. 13a-c to Figs. 13b-
700 d). This effect is particularly evident over the crest of the Gaggiano footwall: the area shown in
701 blue at end Miocene for both middle and late Triassic intervals (fig. 12c & f), corresponding to
702 a transformation ratio of less than 10%, has completely disappeared at present day for the
703 geological heat flow model (fig 13a-c), whilst for the overpressure model narrow belts with low
704 transformation ratio remain over the crest of the footwall region (fig 13b-d).

705 Remarkably, both models show hydrocarbon generation occurring in two phases (Figs
706 11, 12, 13 & 14): a Jurassic phase and an Alpine Tertiary phase, the latter starting in the
707 Oligocene but occurring mainly during the last 5-10 million years, in agreement with earlier
708 findings (Novelli et al., 1987; Mattavelli & Novelli, 1987; Mattavelli et al., 1993; Lindquist,
709 1999; Bertello et al., 2010).

710

711 **Discussion**

712

713 *Overall validity of the thermo-structural modelling approach and choice of the better model*

714 3D charge modelling was carried out for a number of structures within the western Po valley
715 overpressure cell in order to compare model predictions with observed hydrocarbon distribution
716 and properties. Charge modelling was performed using the simple kinetic methodology
717 described in Pepper & Corvi (1995a, 1995b) and Pepper & Todd (1995) as implemented in the
718 Trinity Basin Modelling software. Source rock kerogen types and initial HIs and TOCs are
719 shown in Table 2. For each structure, kitchen areas were defined as the areas of the present-day
720 top Triassic depth map over which buoyancy forces would drain migrated hydrocarbons
721 towards the relevant structural culmination. Those areas were then further refined by
722 superimposing the source rock polygons from the GDE maps. Finally, the charge volumes for
723 the various traps were then limited to those available after the critical moment, i.e., the time at
724 which the trap formed or the seal became able to retain a hydrocarbon column (Fig. 14). The
725 model also incorporates the effect of migration losses along the path to the trap, with considered
726 loss of 0.075 MMbbl/km², derived using the methodology proposed by Mackenzie & Quigley
727 (1988) with a bed thickness of 500m and an average porosity of 1.5%. Reservoir and top-seal
728 parameters are defined in order to allow the basin model to calculate volumes trapped in each
729 structure. Here, a single late Triassic reservoir was modelled as a 250m thick, 100% net-to-
730 gross slab with an average porosity of 3% (see Bello & Fantoni, 2002 for comparison). Top-

731 seal capacity was modelled as 300 pounds per square inch (psi) using simple capillary seal
732 models for pelagic carbonates. The basin model has been re-run, and the following predicted
733 parameters were extracted: volume of charge available from the relevant kitchen area since the
734 critical moment, trapped hydrocarbon volume and gas/oil ratio (GOR) of the trapped fluids.

735 These predicted parameters compare well with estimates of the initially in place
736 hydrocarbon volume (HCIIP) at each trap and for the GOR of the fluids present in the three
737 main discoveries in the western Po valley (Fig.15) : to a first order, both the actual geological
738 heat flow and the reduced heat flow / overpressure models replicate accurately the overall
739 distribution and phase of hydrocarbons and predict significant discoveries at Villafortuna-
740 Trecate and Malossa and a smaller discovery at Gaggiano. They also predict a rich petroleum
741 system with significant volumes of hydrocarbons spilled from traps that have been breached,
742 bypassed and/or overfilled. This is evident at Gaggiano where the two models equally calculate
743 small trapped volumes due to the size of the trap. Indeed, being located at the crest of a regional
744 high (see Figs.2 and 3a), the Gaggiano trap appears to be linked to an extensive kitchen area,
745 which, since the Mid-Miocene critical moment, has generated charge volumes 25 to 50 times
746 larger than the trapped volumes. Finally, the two models predict liquid hydrocarbons with
747 moderate-to-low GOR at Villafortuna-Trecate and Gaggiano whilst high GOR fluids are
748 predicted at Malossa.

749 As a result, despite the relative simplicity of the modelling approach adopted and
750 uncertainties regarding source rock distribution, our 3D thermo-structural modelling provides
751 for the first time a consistent integration of the 3D structures with their thermal histories and
752 reliably simulates the related hydrocarbon maturation/generation process across the entire Po
753 Valley basin.

754 In detail however, the reduced heat flow / overpressure model better matches the
755 observed data than the actual geological heat flow model. In this respect, Figure 15a compares
756 calculated trap HCIIP volumes with the predicted charge available from the kitchen area since
757 the critical moment. The graph shows that predictions from the overpressure model (excluding
758 Gaggiano) correlate better with trap HCIIP values than those from the actual geological heat
759 flow model. Also, the overpressure model can successfully explain the failures in the inversion
760 traps in the Lacchiarella hangingwall (Lacchiarella and San Genesio) and the deep traps east of
761 Malossa (Chiari, Belvedere). Conversely, the actual geological heat flow model predicts
762 significant volumes in several of these traps. Furthermore, charge volumes available to the trap
763 are closer to HCIIP volumes for the overpressure model than for the actual geological heat flow

764 model. This implies that smaller volumes are spilled to shallower traps and/ or stratigraphic
765 levels. Given little evidence for large spilled volumes in the Po Valley, the prediction of smaller
766 excess volumes favours the overpressure model.

767 Figure 15b shows how predicted trap volumes from the basin models compare with the
768 calculated trap HCIIP volumes. Given that traps are generally oversupplied with hydrocarbons
769 in both models, there is relatively little difference in the performance of the two models.
770 However, it is of note that Malossa volumes are matched better by the overpressure model as
771 there is a charge limitation on predicted volumes in the trap; the actual geological heat flow
772 model predicts larger volumes with the trap being oversupplied and excess volumes spilled.
773 Finally, Figure 15c shows that the overpressure model more successfully predicts fluid phase
774 than the actual geological heat flow model, which predicts higher maturity fluids with higher
775 GORs than observed for all three of the main discoveries.

776 We therefore conclude that overpressure as simulated by a reduced heat flow is a viable
777 and valid mechanism that has likely significantly delayed hydrocarbon maturation in the
778 western Po valley, as proposed by earlier authors (Chiaramonte & Novelli, 1986, Carr, 1999).

779

780 *Uncertainties on the modelling results and sensitivity*

781

782 **Structural model uncertainties:** The Po Valley 3D structural model (Turrini et al., 2014)
783 defines the present-day configuration and geometrical framework of the basin. Although a
784 regional scale kinematic restoration to pre-Alpine and/or Mesozoic position has been recently
785 attempted (Turrini et al., 2016), the chosen modelling approach applied here to the evolution of
786 the Mesozoic petroleum system is a conventional one. Although a 2D kinematic approach
787 would have been a more accurate methodology for modeling such a complex petroleum system
788 (Gusterhuber et al., 2014; Neumaier et al., 2014), simple vertical back-stripping was carried out
789 to describe the tectono-stratigraphic evolution of the basin. Despite this simplification, we
790 believe the modelling results are reasonable due to the following considerations.

791 The model has been restricted to the foreland domain, characterized by low deformation
792 and in which vertical displacements are more significant than horizontal ones (Cassano et al.,
793 1986; Turrini et al., 2014). Locally, thrust faults can create a late tectonic over-thickening of
794 the thrust section, particularly where a hangingwall ramp is juxtaposed with a footwall ramp.
795 An example is provided by the Medolo Formation in the Belvedere well, where an estimated
796 500m of tectonic thickening occurs on a Miocene thrust fault. This is incorporated into the
797 model as stratigraphic thickening of the Medolo sediments and contributes to the high

798 transformation ratio in the vicinity of the Belvedere well shown at end Jurassic times (Figs 12a
799 and d). However, sensitivity modelling indicates that the effect is minor and local, given the
800 relatively small scale of the thrusting involved, and does not impact the validity of the regional
801 results presented.

802 The vertical back-stripping approach used approximately describes the recent evolution
803 of the system, and covers the bulk of hydrocarbons generated during the Alpine phase. The
804 model will not adequately describe generation and expulsion of hydrocarbons during the earlier
805 Jurassic phase as trap distribution and geometry were substantially different during this phase.
806 However, the effective charge in both models has been limited to post-critical moment, which
807 took place sometimes in the Miocene. Consequently, hydrocarbons generated earlier are lost to
808 the system and deemed to have leaked to the surface. Therefore, the lack of structural restoration
809 does not impact the results, although any possible re-migration from reactivated Mesozoic traps
810 has not been considered.

811 A further simplification in the model is that all surfaces other than the base Pliocene
812 surface have been modelled as conformities. A number of erosional unconformities earlier in
813 the Tertiary have been neglected, due to insufficient data to simulate these at the regional scale
814 of the model. The literature on the region (Pieri & Groppi, 1981; Cassano et al., 1986; Ghielmi
815 et al., 2012; Rossi et al., 2015) suggests that: a) erosion of Mesozoic sediments was essentially
816 restricted to locally uplifted areas, such as the syn-rift footwall erosion experienced over the
817 crest of the Gaggiano footwall and b) erosion of Tertiary deposits associated with intra-Tertiary
818 unconformities is in the order of few hundred metres. Consequently, given limited pre-Pliocene
819 erosion and high Pliocene-Pleistocene sedimentation rates, it is likely that Mesozoic source
820 rocks are at maximum depth of burial and peak thermal maturity at the present day across the
821 vast majority of the basin (Ghielmi et al., 2012; Rossi et al., 2015). Given the limited and local
822 nature of the pre-Pliocene unconformities, it is considered unlikely that their absence from the
823 model significantly affects results, although it may result in some local errors in the maturation
824 history.

825

826 **Petroleum systems uncertainties:** The main uncertainty pertaining to petroleum systems
827 consists of the source rock distribution (position and areal extent of the source polygons of Fig.
828 8b and c) defined on the basis of the GDE maps. A second major uncertainty refers to the
829 assigned net source thicknesses, essentially due to paucity of the available input data. Indeed,

830 the models mainly rely on outcrop information from the Southern Alps and it should be noted
831 that the South Alpine Front, which separates the outcrops from the subsurface of the Po Valley,
832 is a Tertiary feature with an estimated 50-70 km of shortening (e.g., Handy et al., 2014). In this
833 framework, considerable uncertainty exists in correlating from the outcrop to the
834 subsurface. Furthermore, the source rock distribution defined here includes a number of
835 postulated source basins, particularly in the eastern Po Valley and the Adriatic offshore.
836 Another potential issue arises in the interpretation of the unsuccessful wells in the western Po
837 Valley.

838 The ability to explain these failures as due to lack of access to recent charge was used
839 as a reason for preferring the reduced heat flow / overpressure model to the actual geological
840 heat flow model (the latter predicting the availability of significant recent charge volumes to
841 these traps). Clearly there is a range of other potential failure mechanisms unrelated to source
842 rock that could explain these well results.

843 **Sensitivity to thermal and burial history parameters:** The basin modelling presented here
844 derives from a long and continuous analysis of sensitivities for the many parameters which
845 control the burial and thermal history of the Po Valley region.

846 Heat flow based on data from the available literature (see Fig.10) was chosen as the key
847 element to replicate the overpressure effect. Reducing the heat flow is a straightforward method
848 to control the vitrinite maturation progression around the basin. In addition, using heat flow as
849 a key controlling factor on hydrocarbon maturation can be used as stand-alone tool which does
850 not directly impact the various parameters which affect the simulation process (e.g. rock
851 properties, burial history, source distribution). Quality control (QC) on the heat flow history
852 was concentrated on both past and present history to best match the vitrinite profile available at
853 selected well locations in the Po Valley. In particular, in order to build the reduced heat flow /
854 overpressure model particular attention has been paid to the reconstruction of the Miocene-Plio-
855 Pleistocene curve segment. This needed to be viable with respect to the tectono-stratigraphic
856 history of the basin where rapid sedimentation of the clastic succession was associated with
857 localized overpressure build-up in the Mesozoic carbonates. The radiogenic heat flow
858 component possibly derived from mineral associations of the Tertiary sediment has also been
859 evaluated although it was finally considered irrelevant to the basin model results.

860 Notwithstanding the key role of the Po Valley heat flow on the study objectives, all of
861 the basin model parameters (see Table 2) have been progressively evaluated and implemented

862 from the initial Genesis/Trinity software standard values. Again, the primary aim was to refine
863 the match with the available maturity data while keeping a present-day heat flow consistent
864 with the published one. In particular: a) lithologies have been refined on the basis of a careful
865 analysis of the well logs; b) matrix thermal conductivity of the sediments, especially for shales
866 and sandstones, have been reviewed in the light of the available literature; c) for specific rock
867 types such as silts and conglomerates, surface porosity, compaction coefficient, porosity and
868 bulk density have been adjusted using literature data while iteratively validating the model
869 constraints (i.e. well temperatures and vitrinite profiles); d) porosity in the Mesozoic carbonates
870 was also validated against the field values as it was considered the main variable in the
871 computation of migration losses in the model versus observed hydrocarbon production analysis.

872 Further sensitivity tests were performed on progressive sea level paleodepth variations,
873 an important factor on sea level temperature at the different stages of the burial-thermal history.
874 Indeed, almost all of the decrease in water-sediment interface temperature occurs in the first
875 hundred metres so that anomalously shallow paleodepth estimates can cause 10°C excess
876 temperature at the source rock level through part of the geological burial history. This would
877 then require an unrealistic reduction in the heat flow in order to match the vitrinite data
878 constraining the basin model.

879 Finally, the properties and parameters which have been used and progressively
880 implemented during the model building are strictly interrelated. Sensitivity analyses
881 demonstrated how changing one parameter often results in a compensatory change to another
882 parameter. Their implementation, coupled with heat flow adjustment had a significant impact
883 on the final model results.

884 *Implications for the thermo-structural evolution of the Po basin and hydrocarbon generation* 885 *and prospectivity*

886 The 3D basin model of the Po Valley presented in this paper provides important insights
887 into the geometry and structural evolution of hydrocarbon-bearing traps, and into the generation
888 and migration of hydrocarbons into these traps.

889 The model confirms earlier studies (Novelli et al., 1987; Mattavelli & Novelli, 1987;
890 Mattavelli et al., 1993; Lindquist, 1999; Bertello et al., 2010) and shows that hydrocarbon
891 generation likely occurred in two phases: a Jurassic phase and an Alpine Tertiary phase, the
892 latter occurring mainly during the last 5-10 million years. Our results emphasize the impact that

893 Mesozoic and Tertiary Alpine tectonics had on the development of a successful petroleum
894 system in the Po valley. The Mesozoic extensional phase controlled reservoir and source
895 distribution, trap formation (e.g. Gaggiano oil field) and the early phases of hydrocarbon
896 maturation in subsiding half grabens associated with high heat flows and substantial syn-to
897 early-post-rift sediment accumulation. The Tertiary compressional phase controlled trap
898 formation, either by generating new traps (Cavone oil field) or by reactivating older ones
899 inherited from the Mesozoic extensional phase (Villafortuna-Trecate, Malossa oil fields).
900 Clearly, regional hydrocarbon maturation and expulsion/migration are related to rapid foredeep
901 burial ahead of the evolving southern Alpine and northern Apenninic thrust belts.

902 From a hydrocarbon exploration point of view, the timing of hydrocarbon maturation is
903 favourable for exploration in the western Po Valley. Trap formation is likely to have occurred
904 during the Oligocene to late Miocene, along with significant post-Miocene hydrocarbon
905 generation and expulsion (migration?). In contrast, in the eastern Po Valley, timing is less
906 favourable as traps - Plio-Pleistocene in age - tend to either post-date the main hydrocarbon
907 generation phase, or they formed when generation was not advanced enough for migration to
908 occur, or for traps to be filled.

909

910 **Conclusions**

911 Using the recent Po Valley 3D structural model as an input for basin modelling, the
912 approach presented in this contribution provides for the first time a unique integration of the 3D
913 structures with their thermal history and the related hydrocarbon maturation/generation process
914 across the entire Po Valley basin.

915 When compared with the observed distribution of hydrocarbons, our basin modelling
916 results suggest that, at the regional scale, both maturity models (actual geological heat flow
917 model and reduced heat flow-overpressure model designed to simulate the delaying effect of
918 overpressure on hydrocarbon generation) appear consistent with the observed hydrocarbon
919 distribution. In detail however, the overpressure model a) provides an improved match to
920 observed maturity data, b) provides a better fit between calculated trap HCIIP volumes and
921 predicted charge available from the kitchen area since the critical moment and c) predicts
922 hydrocarbon phase (as measured by GOR) more accurately than the geological heat flow model.
923 However caution should be applied to the different variables and uncertainties which pertain to
924 the accumulation process (i.e. source rock net pay, expelled versus un-movable hydrocarbons,
925 heterogeneity in the TOC content of the source intervals, reservoir net volume and associated

926 heterogeneity, and quantitative estimates of migration losses). The modelling results confirm
927 that the delaying effect of overpressure is an important factor to be taken into account in
928 predictions of hydrocarbon maturation and generation.

929 The study also confirms the impact that Mesozoic and Tertiary Alpine tectonics had on
930 the development of a successful petroleum system in the Po valley. The Mesozoic extensional
931 phase controlled reservoir and source distribution, trap formation and the early phases of
932 hydrocarbon maturation in subsiding half grabens associated with high heat flows and
933 substantial syn-to early-post-rift sediment accumulation. The Tertiary compressional phase
934 controlled trap formation, either by generating new traps or by reactivating older ones inherited
935 from the Mesozoic extension.

936 This study demonstrates the utility and applicability of a consistent integrated 3D model
937 of the thermo-structural history of sedimentary basins to constrain the geometry and structural
938 evolution of hydrocarbon-bearing traps as well as the generation and migration of hydrocarbons
939 into these traps.

940

941 Acknowledgements

942 Roberto Fantoni from ENI S.p.a. is kindly acknowledged for discussion about some parts of the
943 manuscript. We thank Jo Prigmore, Tim Diggs and Ozkan Huvaz for their constructive
944 comments on the manuscript.

945

946 References

947 Andreatta, C., Dal Piaz, G., Vardabasso, S., Fabiani, R., Dal Piaz, G., 1957. Carta geologica
948 delle Tre Venezie, scale 1:100,000, Map “10-Bolzano”.

949 Assereto, R., Jadoul, F., Omenetto, P., 1977. Stratigrafia e metallogenese del settore occidentale
950 del distretto a Pb, Zn, fluorite e barite di Gorno (Alpi bergamasche) - Riv. Ital. Paleont., 83, 3,
951 395-532.

952 Bello, M., Fantoni, R., 2002. Deep oil plays in the Po Valley: Deformation and hydrocarbon
953 generation in a deformed foreland – AAPG HEDBERG CONFERENCE, “Deformation
954 History, Fluid Flow Reconstruction and Reservoir Appraisal in Foreland Fold and Thrust Belts”
955 May 14-18, 2002, Palermo – Mondello (Sicily, Italy).

956 Berra, F., Carminati, E., 2010. Subsidence history from a backstripping analysis of the Permo-
957 Mesozoic succession of the Central Southern Alps (Northern Italy). Basin Research, 22, 952-
958 975.

- 959 Berra F., Galli M.T., Reghellin F., Torricelli S., Fantoni R., 2009. Stratigraphic evolution of the
960 Triassic-Jurassic succession in the Western Southern Alps (Italy) : the record of the two-stage
961 rifting on the distal passive margin of Adria– Basin Research, 21, 335-353.
- 962 Bersezio, R. & Bellantani, G., 1997. The thermal maturity of the Southalpine mesozoic
963 succession north of Bergamo by vitrinite reflectance data. Atti Tic.Sc.Terra, 5, 101-114.
- 964 Bertello. F., Fantoni, R., Franciosi, R., Gatti, V, Ghielmi, M., Pugliese, A., 2010. From thrust-
965 and-fold belt to foreland: hydrocarbon occurrences in Italy. VINING, B.A. & PICKERING, S.
966 C. (eds) Petroleum Geology: From Mature Basins to New Frontiers – Proceedings of the 7th
967 Petroleum Geology Conference, 113–126. DOI: 10.1144/0070113 # Petroleum Geology
968 Conferences Ltd. Published by the Geological Society, London.
- 969 Bertotti G., Picotti V., Bernoulli D., Castellarin A.,1993. From rifting to drifting: tectonic
970 evolution of the South-Alpine upper crust from the Triassic to the Early Cretaceous –
971 Sedimentary Geology, 86, 53-76.
- 972 Bongiorno, D., 1987. La ricerca di idrocarburi negli alti strutturali mesozoici della Pianura
973 Padana: l’esempio di Gaggiano – Atti Tic. Sc. Terra Vol. XXXI, pp. 125-141.
- 974 Brack, P., Rieber, H., 1993. Towards a better definition of the Anisian/Ladinian boundary :
975 New biostratigraphic data and correlations of boundary sections from the Southern Alps.
976 Eclogae geol. Helv. 86/2: 415-527. (FINE BY ME)
- 977 Braga, Gp., Castellarin, A., Corsi, M., De Vecchi, Gp., Gatto, Gino., Gatti, Giuseppe,
978 Largaiolli, T., Monese, A., Mozzi, G., Rui, A., Sassi, F.P., Zirpoli, G., 1968. Carta Geologica
979 D’Italia, scale 1:100,000, Map “36-Schio”.
- 980 Burnham, A.K., and Sweeney, J.J., 1989, A chemical kinetic model of vitrinite maturation and
981 reflectance: Geochimica et Cosmochimica Acta, v. 53, p. 2649–2657.
- 982 Calabrò R., Ceriani A., Di Giulio A., Fantoni R., F. Lino, Scotti P, 2003. Thermal history of
983 syn-rift successions between the Iseo Basin and the Trento Plateau: results from the integrated
984 study of organic matter maturity and fluid inclusions. Atti Tic. Sc. Terra, serie sp. v. 9, pp. 88-
985 91.
- 986 Cantelli, C., Carloni, G.C., Castellarin, A., Ceretti, E., Colantoni, P., Cremonini, G., Elmi, C.,
987 Frascari, F., Monesi, F., Pisa, G., Rabbi, E., Tomadin, L., Vai, G.B., Braga, Gp., Corsi, M.,
988 Gatto, G., Locatelli, D., Rui, A., Sassi, P., Zirpoli, G., Dal Cin, R., Largaiolli, T., Gatto, G.O.,
989 1971. Carta Geologica D’Italia, scale 1:100 000, Map “4C-13- Monte Cavallino-Ampezzo”.
- 990 Carannante, S., Argnani, A., Augliera, P., Cattaneo, M., D’Alema, E., Franceschina, G., Lovati,
991 S., Massa, M., Monachesi, G., Moretti, M., 2014. Risultati da Progetto Sismologico S1 (INGV-
992 DPC 2013) Base-knowledge improvement for assessing the seismogenic potential of Italy
993 Section n: D18/b2 Relocated seismicity in the Po Plain. Workshop Terremoto Emilia 2012,
994 Roma 26 Maggio 201.

- 995 Carminati, E., Doglioni, C., 2012. Alps vs. Apennines: the paradigm of a tectonically
996 asymmetric Earth. *Earth-Science Reviews*, 112, 67-96.
- 997 Carminati, E., Cavazza, D., Scrocca, D., Fantoni, R., Scotti, P., Doglioni, C., 2010. Thermal
998 and tectonic evolution of the southern Alps (northern Italy) rifting: Coupled organic matter
999 maturity analysis and thermokinematic modelling. *AAPG Bulletin*, v. 94, no. 3 (March 2010),
1000 pp. 369–397.
- 1001 Carr, A.D., 1999. A vitrinite reflectance kinetic model incorporating overpressure retardation.
1002 *Marine and Petroleum Geology*, 16, 355-377.
- 1003 Carulli, G.B., Salvador, G.L., Ponton, M., Podda, F., 1997. La dolomia di forni: evoluzione di
1004 un bacino euxinico tardo triassico nelle prealpi carniche. *Boll. Soc. Geol. It.*, 116, 95-107.
- 1005 Casati, P., Assereto, R., Comizzoli, G., Passeri, L.D., Boni, A., Cassinis, G., Cerro, A., Rosetti,
1006 R., Accordi, B., Dieni, I., Malaroda, R., Bianchi, A., Cevalas, G., Dal Piaz, Gb., Morgante, S.,
1007 1970. *Carta Geologica D'Italia scale 1:100,000, Map "34- Breno"*.
- 1008 Casero, P., 2004. Structural setting of petroleum exploration plays in Italy. In Crescenti, V.,
1009 D'Offizi, S., Merlino, S., Sacchi, L. (Eds), *Geology of Italy. Special Volume of the Italian*
1010 *Geological Society for the IGC 32nd, Florence*, 189-199.
- 1011 Cassano, E., Anelli, L., Fichera, R., Cappelli, V., 1986. Pianura Padana, interpretazione
1012 integrata di dati Geofisici e Geologici. - 73° congresso Soc. Geol. It., Roma.
- 1013 Castellarin, A., Vai, G.B., 1982. Introduzione alla geologia strutturale del Sudalpino. In:
1014 Castellarin, A., Vai, G.B., - *Guida alla geologia del Sudalpino centro orientale. Guide Geol. Reg.*,
1015 *Soc. Geol. It.*, 1-22.
- 1016 Castellarin A., Eva C., Giglia G., Vai G.B., Rabbi E., Pini G.A. & Crestana G., 1985. Analisi
1017 strutturale del Fronte Appenninico Padano. *Giornale di Geologia*, 47, pp.47-75.
- 1018 Castellarin, A., 2001. Alps-Apennines and Po Plain-Frontal Apennines relationships. In: VAI
1019 G. B. & MARTINI I. P. (Eds.), *Anatomy of an Orogen. The Apennines and adjacent*
1020 *Mediterranean Basins*, Kluwer, London, 177- 196.
- 1021 Castiglioni, B., Leonardi, P., Merla, G., Trevisan, S., Zenari, S., 1940. *Carta geologica delle Tre*
1022 *Venezie, scale 1:100,000, Map "12- Pieve di Cadore"*.
- 1023 Castiglioni, B., Boyer, G., Leonardi, P., Venzio, S., Dal Piaz, G., Vialli, V., Zenari, S., 1941.
1024 *Carta geologica delle Tre Venezie, scale 1:100,000, Map "23- Belluno"*.
- 1025 Cati, A., Sartorio, D., Venturini, S., 1987. Carbonate platforms in the subsurface of the northern
1026 Adriatic area. *Mem. Soc. Geol. It.*, v.40. pp. 295-308.
- 1027 Ciarapica, G., Cirilli, S., D'Argenio, B., Marsella, E., Passeri, L., Zaninetti, L., 1986. Late
1028 Triassic open and euxinic basins in Italy. *Rend. Soc. Geol. It.*, 9, pp.157-166.

- 1029 Chiamonte, M.,A., Novelli, L., 1986. Organic matter maturation in Northern Italy: some
1030 determining agents. *Org. Geochem.*, 10, 281-290.
- 1031 Dal Piaz, G., Venzo,S., Fabiani, R., Trevisan, L., Pia, J., 1946. Carta geologica delle Tre
1032 Venezie, scale 1:100,000, Map “37-Bassano del Grappa”.
- 1033 Defant, A., 1961. *Physical Oceanography*, Vol. 1, Pergamon Press, 728 pp.
- 1034 Della Vedova, B., Bellani, S., Pellis, G., Squarci, P., 2001. Deep temperatures and surface heat
1035 flow distribution. In: VAI G.B. & MARTINI I.P. (Eds.): “Anatomy of an orogen: the
1036 Apennines and adjacent Mediterranean basins”. Kluwer Academic Publishers: 65-76,
1037 Dordrecht, The Netherlands.
- 1038 Desio, A., Venzo, S., 1954. Carta Geologica D'Italia, scale 1:100,000, Map “33- Bergamo”.
- 1039 Dewey, J.F.; Pitman, C., Ryan, B. F., Bonnin, J. 1973. Plate tectonics and the evolution of the
1040 Alpine systems. *Geological Society of America Bulletin*, 84, 3,137-80.
- 1041 De Zanche, V., Gianolla, P., Roghi, G., 2000. Carnian stratigraphy in the Raibl/Cave del Predil
1042 area (Julian Alps, Italy). *Eclogae. Geol. Helv.*, 93, 331–347.
- 1043 Doglioni, C., Bosellini, A., 1987. Eo-Alpine and meso-Alpine tectonics in the Southern Alps.
1044 *Geol. Rundsch.* 76 (3), 735–754.
- 1045 Di Giulio, A., Mancin, N., Martelli, L., Sani, F., 2013. Foredeep palaeobathymetry and
1046 subsidence trends during advancing then retreating subduction: the Northern Apennine case
1047 (Oligocene-Miocene, Italy). *Basin Research* (2013) 25, 260–284, doi: 10.1111/bre.12002.
- 1048 Errico, G., Groppi, G., Savelli, S., Vaghi G.C., 1980. Malossa Field: a deep discovery in the Po
1049 Valley, Italy – AAPG Memoir 30, 525-538.
- 1050 Fantoni, R., Bello, M., Ronchi, P., Scotti, P., 2002. Po Valley oil play – From the Villafortuna-
1051 Trecate field to South Alpine and Northern Apennine exploration. EAGE 64th Conference &
1052 Exhibition — Florence, Italy, 27 - 30 May 2002.
- 1053 Fantoni, R., Scotti, P., 2003. Thermal record of the Mesozoic extensional tectonics in the
1054 Southern Alps – *Atti Ticinensi di Scienze della Terra* 9, 96-101.
- 1055 Fantoni, R., Decarus, A., Fantoni E., 2003. Mesozoic extension at the Western margin of the
1056 Southern Alps (Northern Piedmont, Italy) – *Atti Ticinensi di Scienze della Terra* 44, 97-110.
- 1057 Fantoni, R., Bersezio, R., Forcella, F., 2004. Alpine structure and deformation chronology at
1058 the Southern Alps-Po Plain border in Lombardy. *Boll.Soc.Geol.It.*, 123 (2004), 463-476.
- 1059 Fantoni R., Franciosi R., 2010. Tectono-sedimentary setting of the Po Plain and Adriatic
1060 foreland - *Rend.Fis.Acc.Lincei*, 21, (Suppl 1):S197-S209, DOI 10.1007/s12210-010-0102-4.

- 1061 Franciosi R. & Vignolo A., 2002. Northern Adriatic foreland- a promising setting for the south
1062 Alpine Mid-Triassic Petroleum system. EAGE 64th Conference & Exhibitions, Florence, Italy,
1063 27-30May 2002.
- 1064 Galli, M.T., Jadoul, F., Bernasconi, S.M., Cirilli, S., Weissert, H., 2007. Stratigraphy and
1065 palaeoenvironmental analysis of the Triassic-Jurassic transition in the western Southern Alps
1066 (Northern Italy). *Palaeogeography, Palaeoclimatology, Palaeoecology*, 44, 52-70
- 1067 Gatto, G.O., Gatto, P., Baggio, P., De Vecchi, Gp., Mezzacasa, G., Piccirillo, E., Zirpoli, G.,
1068 Friz., Gatto, G., Corsi, M., Sassi, F.P., Monese, A., Gregnanin, A., Zilian, T., Largaiolli, T.,
1069 1969. Carta Geologica D'Italia, scale 1:100,000, Map "1 & 4A- Passo del Brennero and
1070 Bressanone".
- 1071 Gatto, P., Rui, A., Dal Pra, A., De Zanche, V., Gatto, G., Gatto, G.O., Corsi, M., Nardin, M.,
1072 Sacerdoti, M., Largaiolli, T., Ghezzi, C., D'Amico, C., 1968. Carta Geologica D'Italia, scale
1073 1:100,000, Map "21-Trento".
- 1074 Ghielmi, M., Minervini, M., Nini, C., Rogledi, S., Rossi, M., 2012. Late Miocene-Middle
1075 Pleistocene sequences in the Po Plain and the Northern Adriatic Sea (Italy): The stratigraphic
1076 record of modification phases affecting a complex foreland basin. *Marine and Petroleum
1077 Geology*, [http://dx.doi.org/ 10.1016/j.marpetgeo.2012.11.007](http://dx.doi.org/10.1016/j.marpetgeo.2012.11.007).
- 1078 Gianolla, P., De Zanche, V., Mietto, P., 2012. Triassic sequence stratigraphy in the Southern
1079 Alps (Northern Italy): definition of sequences and basin evolution. *SEPM Special Publication
1080 No. 60*, ISBN 1-56576-043-3.
- 1081 Gnaccolini, M., Jadoul, F., 1990. Carbonate platform, lagoon and delta "high-frequency" cycles
1082 from the Carnian of Lombardy (Southern Alps, Italy). *Sedimentary Geology*, 67, 143-159.
- 1083 Gortani, M., Desio, A., 1925. Carta geologica delle Tre Venezie, scale 1:100,000, Map "14-
1084 Pontebba".
- 1085 Greber, E., W. Leu, D. Bernoulli, M. Schumacher, and R. Wyss, 1997. Hydrocarbon provinces
1086 in the Swiss southern Alps—A gas geochemistry and basin modelling study. *Marine and
1087 Petroleum Geology*, v. 14, p. 3–25, doi:10.1016/S0264-8172(96)00037-2.
- 1088 Gretner, P.E., 1981. Geothermics: using temperature in hydrocarbon exploration. AAPG, Short
1089 Course Notes, 17.
- 1090 Grobe, A., Littke, R., Sachse, V., Leythaeuser, D., 2015. Burial history and thermal maturity of
1091 Mesozoic rocks of the Dolomites, Northern Italy. *Swiss Geological Society*, doi
1092 10.1007/s00015-015-0191-2.
- 1093 Gusterhuber, J., Hinsch, R., Sachsenhofer, R.F., 2014. Evaluation of hydrocarbon generation
1094 and migration in the Molasse fold and thrust belt (Central Eastern Alps, Austria) using structural
1095 and thermal basin models. *AAPG Bulletin*, v. 98, no. 2, pp. 253–277.

- 1096 Handy, R., Ustaszewski, K., Kissling, E., 2014. Reconstructing the Alps-Carpathians-Dinarides
1097 as a key to understanding switches in subduction polarity, slab gaps and surface motion.
1098 International Journal of Earth Science (Geol Rundsch) - DOI 10.1007/s00531-014-1060-3.
- 1099 Jadoul, F. 1986, Stratigrafia e Paleogeografia del Norico nelle Prealpi bergamasche occidentali.
1100 Riv.It.Paleont.Strat, v.91,n.4 pp.479-512.
- 1101 Jadoul, F., Berra F. 7 Frisia, S., 1992. Stratigrafic and palaeogeographic evolution of a
1102 carbonate platform in an extensional tectonic regime:the example of the Dolomia Principale in
1103 Lombardy (Italy). Riv.It.Paleont.Strat., v.98,n.1,pp.29-44.
- 1104 Jadoul, F., Nicora A., Ortenzi A., Pohar C., 2002. Ladinian stratigraphy and palaeogeography
1105 of the Southern Val Canale (Pontebbano-Tarvisiano, Julian Alps, Italy). Mem Soc.geol It., v57,
1106 pp29-43.
- 1107 Jarvie, D.M., Claxton, B.L., Henk, F., Breyer, J.T., 2001. Oil and Shale Gas from the Barnett
1108 Shale, Ft. Worth Basin, Texas, AAPG National Convention, June 3-6, 2001, Denver, CO,
1109 AAPG Bull. Vol. 85, No. 13 (Supplement), p.A100.
- 1110 Katz, B.J., Dittmar, E.I., Ehret, G.E., 2000. A geochemical review of carbonate source rocks in
1111 Italy. Journal of Petroleum Geology, v.23 (4), pp.399-424.
- 1112 Keim, L., Spötl, C., and Brandner, R., 2006. The aftermath of the Carnian carbonate platform
1113 demise: a basinal perspective (Dolomites, Southern Alps): Sedimentology, v. 53 p. 361-386,
1114 doi: 10.1111/j.1365-3091.2006.00768.x.
- 1115 Lindquist, S.J., 1999. Petroleum systems of the Po Basin province of northern Italy and the
1116 northern Adriatic Sea; U.S. Geological Survey Open-File Report 99-50-M, 19 p., 15 figs., 3
1117 tables.
- 1118 Lipparini, T., Perrella, G., Mediolio, F., Venzo,S., Barbier, F., Malaroda, R., Sturani, C., Carraro,
1119 F., Zanella, E., Corsi, M., Gatto, G., Piccoli, G., 1969. Carta Geologica D'Italia, scale
1120 1:100,000, Map "48-Peschiera del Garda".
- 1121 Mackenzie, A. S., & Quigley, T. M. (1988). Principles of geochemical prospect appraisal.
1122 AAPG Bulletin, 72(4), 399-415.
- 1123 Mann, D. M., Mackenzie, A. S., 1990. Prediction of pore fluid pressures in sedimentary basins:
1124 Marine and Petroleum Geology, 7, no. 1, 55-65, [http://dx.doi.org/10.1016/0264-](http://dx.doi.org/10.1016/0264-8172(90)90056-M)
1125 [8172\(90\)90056-M](http://dx.doi.org/10.1016/0264-8172(90)90056-M).
- 1126 Masetti, D., Fantoni, R., Romano, R., Sartorio, D., Trevisani, E., 2012. Tectonostratigraphic
1127 evolution of the Jurassic extensional basins of the eastern southern Alps and Adriatic foreland
1128 based on an integrated study of surface and subsurface data. AAPG Bulletin, v. 96, no. 11, pp.
1129 2065-2089.
- 1130 Mattavelli, L., Novelli, L., 1987. Origin of the Po basin hydrocarbons – Mémoires de la Société
1131 Géologique de France, nouvelle série. 151; 97-106.

- 1132 Mattavelli, L., Margarucci, V., 1992. Malossa Field – Italy, Po Basin, in Foster, N.H., and
1133 Beaumont, E.A., Treatise of Petroleum Geology, Atlas of Oil and Gas Fields, Structural Traps
1134 VII: Tulsa, OK, American Association of Petroleum Geologists, p. 119-137.
- 1135 Mattavelli, L., Pieri, M., Groppi, G., 1993. Petroleum exploration in Italy: a review. *Marine and*
1136 *Petroleum Geology*, 10, 410-425.
- 1137 Mattiolo, E. Novarese, V., Franchi, S., Stella, A., 1927. Carta Geologica D'Italia, scale 1:100
1138 000, Map “30- Varallo”.
- 1139 Michetti, A.M., Giardina, F., Livio, F., Mueller, K., Serva, L., Sileo, G., Vittori, E., Devoti, R.,
1140 Riguzzi, F., Carcano, C., Rogledi, S., Bonadeo, L., Brunamonte, F., Fioraso, G., 2013. Active
1141 compressional tectonics, Quaternary capable faults, and the seismic landscape of the Po Plain
1142 (northern Italy). *Ann. Geophys.* 55 (5), 969–1001, doi:10.4401/ag-5462.
- 1143 Middleton M. (1993) A transient method of measuring the thermal properties of rocks.
1144 *Geophysics*, 58, 357-365.
- 1145 Nardin, M., Rossi, D., Somnavilla, E., Largaiolli, T., Mozzi, G., Gregnanin, A., Zulian, T.,
1146 Zirpoli, G., Corsi, M., Gatto, G.O., Gatto, P., Graga, Gp., Rui, a., 1970. Carta Geologica
1147 D'Italia, scale 1:100,000, Map “22- Feltre”.
- 1148 Nardon, S., Marzorati, D., Bernasconi, A., Cornini, S., Gonfalini, M., Mosconi, S., Romano,
1149 A., Terdich, P., 1991. Fractured carbonate reservoir characterization and modelling a
1150 multidisciplinary case study from the Cavone oil field, Italy: *First Break*, 9, 12, 553-565.
- 1151 Neumaier, M., Littke, R., Hantschel, T., Maerten, L., Joonnekindt, T., Kukla, P., 2014.
1152 Integrated charge and seal assessment in the Monagas fold and thrust belt of Venezuela. *AAPG*
1153 *Bulletin*, v. 98, no. 7, pp. 1325–1350.
- 1154 Novelli, L., Chiaramonte, M. A., Mattavelli, L., Pizzi, G., Sartori, L., Scotti, P., 1987. Oil
1155 habitat in the northwestern Po Basin, in B. Doligez, ed., *Migration of hydrocarbons in*
1156 *sedimentary basins*: Paris, Editions Technip, p. 27–57.
- 1157 Pasquale, V., Gola, G., Chiozzi, P., Verdoya, M., 2011. Thermophysical properties of the Po
1158 Basin rocks. *Geophys. J. Int.*, 186, 69–81. doi: 10.1111/j.1365-246X.2011.05040.x
- 1159 Pasquale, V., Chiozzi, P., Verdoya, M., Gola, G., 2012. Heat flow in the Western Po Basin and
1160 the surrounding orogenic belts. *Geophys. J. Int.*, 190, 8–22. doi: 10.1111/j.1365-
1161 246X.2012.05486.x.
- 1162 Passeri, L.D., Comizzoli, G., Assereto, R., 1967. Carta Geologica D'Italia, scale 1:100,000,
1163 Map “14 A- Tarvisio”.
- 1164 Pepper, A. S., Corvi, P.J., 1995a. Simple kinetic models of petroleum formation. Part I: Oil and
1165 Gas generation from kerogen. *Marine and Petroleum Geology*, v. 12, no. 3, p. 291-319.
- 1166 Pepper, A. S., Corvi, P.J., 1995b. Simple kinetic models of petroleum formation. Part III:
1167 Modelling an open system. *Marine and Petroleum Geology*, v. 12, no. 4, p. 417-452.

- 1168 Pepper, A.S., Dodd, T.A., 1995. Simple kinetic models of petroleum formation. Part II : oil-gas
1169 cracking. *Marine and Petroleum Geology*, v. 12, no. 3, p. 321-340.
- 1170 Pieri, M., Groppi, G., 1981. Subsurface geological structure of the Po Plain, Italy. *Prog. Fin.*
1171 *Geodinamica CNR*, pubbl.414, Roma, 1-113.
- 1172 Pieri M., 1984. Storia delle ricerche nel sottosuolo padano fino alle ricostruzioni attuali – Cento
1173 anni di geologia Italiana, Volume Giubilare, 1° Centenario della Soc.Geol.Ital. 1881-1981,
1174 Roma, 155-177.
- 1175 Pieri, M., 2001, Italian petroleum geology- In: G.B.Vai and I.P. Martini (eds), *Anatomy of an*
1176 *Orogen: the Apennines and Adjacent Mediterranean Basins*, pp.533-550.
- 1177 Pietro, B., Raffaele, D., & Diego, G. (1979, January 1). *Deep Drilling In Po Valley : Planning*
1178 *Criteria And Field Results*. Society of Petroleum Engineers. doi:10.2118/7847-MS
- 1179 Pfiffner, A., 2014. *Geology of the Alps*. Wiley Blackwell, pp. 368.
- 1180 Ponton, M., 2010. *Architettura delle Alpi Friulane*. Museo Friulano di Storia Naturale, Publ.
1181 N° 52, Udine, ISBN 9788888192529.
- 1182 Ravaglia, A., Seno, S., Toscani, G., Fantoni, R., 2006. Mesozoic extension controlling the
1183 Southern Alps thrust front geometry under the Po Plain, Italy: Insights from sandbox models.
1184 *Journal of Structural Geology* 28, 2084-2096.
- 1185 Rigo, F., 1991, Italy to open ‘exclusive’ Po basin area in 1992. *Oil and Gas Journal*, v. 89, no.
1186 21 102-106.
- 1187 Riva, A., Salvatori, T., Cavaliere, R., Ricchiuto, T., Novelli, L., 1986. Origin of oils in Po
1188 Valley, Northern Italy – *Organic Geochemistry*, 10, 391-400.
- 1189 Rossi, M., Minervini, M., Ghielmi, M. & Rogledi, S., 2015. Messinian and Pliocene erosional
1190 surfaces in the Po Plain-Adriatic Basin: Insights from allostratigraphy and sequence
1191 stratigraphy in assessing play concepts related to accommodation and gateway turnarounds in
1192 tectonically active margins. *Marine and Petroleum Geology*, 66, 192-216.
- 1193 Sassi, F.P., Zirpoli, G., Nardin, M., Sacerdoti, M., Bosellini, A., Largaiolli, T., Leonardi, P.,
1194 Somnavilla, E., Mozzi, G., Rossi, D., Proto Decima, F., Dal Monte, M., Paganelli, L., Simboli,
1195 G., Gatto, P., 1970. *Carta Geologica D’Italia*, scale 1:100,000, Map “11- M. Marmolada”.
- 1196 Scotti, P., 2005. Thermal constraints suggested by the study of the organic matter and thermal
1197 modelling strategies: A case history from the southern Alps: *Atti Ticinensi di Scienze della*
1198 *Terra, Serie Speciale*, v. 10, p. 21–35.
- 1199 Scotti, P., Fantoni, R., 2008. Thermal modelling of the extensional Mesozoic succession of the
1200 Southern Alps and implications for oil exploration in the Po Plain foredeep. 70th EAGE
1201 *Congrence & Exhibition – Rome, Italy, 0-12 June, 2008*.
- 1202 Sekiguchi, K., 1984. A method for determining terrestrial heat flow in oil

- 1203 basinal areas. *Tectonophysics*, 103, 67-76
- 1204 Shonborn, G., 1992. Alpine tectonics and kinematics of the central Southern Alps. *Memorie di*
1205 *Scienze Geologiche*; vol XLIV, pp. 229-393.
- 1206 Shonborn, G., 1999. Balancing cross sections with kinematic constraints: the Dolomites
1207 (northern Italy). *Tectonics*, 18, 3, pp. 527-545.
- 1208 Stefani, M., and Burchell, M., 1990. Upper Triassic (Rhaetic) argillaceous sequences in
1209 northern Italy: depositional dynamics and source potential, *in* Hue, A.Y., (Eds.), *Deposition of*
1210 *Organic Facies*, AAPG Studies in Geology #30: Tulsa, OK, American Association of Petroleum
1211 Geologists, p. 93-106.
- 1212 Sweeney, J.J., and Burnham, A.K., 1990. Evaluation of a simple model of vitrinite reflectance
1213 based on chemical kinetics: *American Association of Petroleum Geologists Bulletin*, v. 74, p.
1214 1559-1570.
- 1215 Tissot, B. P., and D. H. Welte, 1984, *Petroleum formation and occurrence*, 2nd ed: New-York,
1216 Springer Verlag, 699 p.
- 1217 Turrini, C., Lacombe, O., Roure, F., 2014. Present-day 3D structural model of the Po Valley
1218 basin, Northern Italy. *Marine and Petroleum Geology* 56, 266-289.
- 1219 Turrini, C., Angeloni, P., Lacombe, O., Ponton, M., Roure, F., 2015. Three-dimensional
1220 seismo-tectonics in the Po Valley basin, northern Italy. *Tectonophysics*, 661, 156-179.
1221 <http://dx.doi.org/10.1016/j.tecto.2015.08.033>.
- 1222 Turrini, C., Toscani, G., Lacombe, O., Roure, F., 2016. Influence of structural inheritance on
1223 foreland-foredeep system evolution: an example from the Po Valley region (northern Italy).
1224 *Marine and Petroleum Geology*, 77, 376-398.
- 1225 Vaghi, G.C., Torricelli, L., Pulga, M., Giacca, D., Chierici, G.L., and Bilgeri, D., 1980,
1226 Production in the very deep Malossa field, Italy: *Proceedings 10th World Petroleum Congress*,
1227 Bucharest, v. 3, p. 371-388
- 1228 Vannoli, P., Burrato, P., Valensise, G., 2014. The seismotectonics of the Po Plain (northern
1229 Italy): tectonic diversity in a blind faulting domain. *Pure Appl. Geophys.*, doi:10.1007/s00024-
1230 014-0873-0.
- 1231 Waples, D.W., Waples, J.S., 2004 A review and evaluation of specific heat capacities of rocks,
1232 minerals, and subsurface fluids. Part 2, fluids and porous rocks. *Nat Resour Res* 13:123-130.
- 1233 Winterer, E. L., Bosellini, A., 1981. Subsidence and sedimentation on Jurassic passive
1234 continental margin, southern Alps, Italy: *AAPG Bulletin*, v. 65, p. 394-421.
- 1235 Wygrala, B.P., 1988. Integrated computer-aided basin modelling applied to analysis of
1236 hydrocarbon generation history in a Northern Italian oil field. *Advances in Organic*
1237 *Geochemistry*, 13, 1-3, pp. 187-197.

1238 Zou Yan-Rong, Peng Ping'an, 2001. Overpressure retardation of organic-matter maturation : a
1239 kinetic model and its application. *Marine and Petroleum Geology*, 18, 707-713.

1240 Zappaterra, E., 1994. Source-Rock distribution Model of the Periadriatic Region. *AAPG*
1241 *Bulletin*, v.78, n.3, pp.333-35.

1242 Zattin, M., Cuman, A., Fantoni, R., Martin, S., Scotti, P., Stefani, C., 2006. From middle
1243 Jurassic heating to Neogene cooling: the thermochronological evolution of the Southern Alps.
1244 *Tectonophysics*, 414, 191-202.

1245

1246 Figure Captions & Tables

1247 Fig.1 – Regional setting, tectono-stratigraphic framework and petroleum system of the Po
1248 Valley basin: a) location map of the study area , major oil fields at Mesozoic level and major
1249 cities (Mi = Milano, To = Torino, Ge = Genova, Ve = Venezia); a=Milan tectonic arc, b=Monferrato
1250 arc, c= Emilia arc, d=Ferrara arc; 1 = Insubric line, 2=Giudicarie line, 3=Schio-Vicenza line,
1251 4=Sestri-Voltaggio line; b) Structural cross section (red dashed line in “a”) through study area
1252 showing present day geometries of main structural elements and hydrocarbon distribution; c)
1253 major stratigraphic units, stratigraphy and hydrocarbon distribution: yellow circle is mainly
1254 biogenic gas; red circle is thermogenic oil in Tertiary successions; green circle is thermogenic
1255 oil & condensate in Triassic carbonates

1256

1257 Fig.2 – Grid showing depth to Top Mesozoic Carbonates (referenced to mean sea level,
1258 contouring every 500 m; bold black lines are major faults at the top of the Mesozoic carbonates);
1259 Purple lines “a” and “b” show the location of the cross-sections in Figure 3. GFz = Giudicarie
1260 Fault zone trend line (thick stippled line) separating the eastern domain from the western
1261 domain; thin stippled white line marks the area covered by the basin modelling study described
1262 in this paper; bold red line represents overpressure cell suggested by Chiaramonte & Novelli
1263 (1986); Major cities: Mi = Milano, To = Torino, Ge = Genova, Ve = Venezia.

1264

1265 Fig.3 – a, b = regional cross-sections through the 3D Po Valley structural model and main
1266 tectonic units; c = cross-section location map at top Mesozoic Carbonate level (see Fig.2 for
1267 larger view).

1268

1269

1270 Fig.4 – The Villafortuna oil-field structure (see location in Figs.1 and 2): a) top Mesozoic depth
1271 grid; RF = Romentino thrust front; b) 3D structural model of the field structure, c) and d) cross-
1272 sections through the 3D model. R/Sr = Reservoir and Source; Sl = Seal; RF = Romentino thrust
1273 front. Note: the Romentino unit geometry within the Oligo-Miocene section in Fig.4c & 4d is
1274 sketched from Pieri & Groppi, 1981, Cassano et al., 1986, Bello & Fantoni, 2002.

1275
1276 Fig.5 – The Gaggiano oil-field and the Lacchiarella structure (see location in Figs.1 and 2): a)
1277 top Mesozoic depth grid, b) 3D structural model of the field and the surrounding structures, c),
1278 d) and e) cross-sections through the 3D model. R/Sr = Reservoir and Source; Sl = Seal. Note:
1279 the extensional terraces in the footwall of the Lacchiarella inverted fault (dotted-lines) are
1280 sketched based on Cassano et al., 1986, Bongiorni, 1987, Fantoni et al.2004.

1281
1282 Fig.6 – The Malossa oil-field region (see location in Figs.1 and 2): a) top Mesozoic depth grid,
1283 b) 3D structural model of the field and the surrounding structures, c), d) and e) cross-sections
1284 through the 3D model. R/Sr = Reservoir and Source; Sl = Seal. Belvedere well is projected onto
1285 section.

1286 Fig. 7 – The Cavone oil-field structure (see location in Figs.1 and 2): a) top Mesozoic depth
1287 grid, b) 3D structural model of the field and the surrounding structures, c), d) and e) cross-
1288 sections through the 3D model. R/Sr = Reservoir and Source; Sl = Seal. Note: the stippled
1289 segments inside the Cavone thrust-related stack are cross-faults sketched from Nardon et al.,
1290 1991.

1291
1292 Fig.8 – Lithostratigraphy and sediment distribution: a) Triassic-Liassic chrono-stratigraphy of
1293 the Po Valley region highlighting the main source rock intervals; b) Gross depositional
1294 environment (GDE) map of the Anisian to late Carnian sediments; c) Gross depositional
1295 environment map of the late Carnian-early Liassic sediments. Data source : Gortani & Desio,
1296 1925; Mattiolo et al., 1927; Castiglioni et al., 1940 and 1941; Dal Piaz et al., 1946; Desio &
1297 Venzo, 1954; Andreatta et al., 1957; Passeri et al., 1967; Braga et al., 1968; Gatto et al., 1968
1298 and 1969; Lipparini et al., 1969; Casati et al., 1970; Nardin et al., 1970; Sassi et al., 1970 ;
1299 Cantelli et al., 1971; Castellarin & Vai, 1982; Jadoul, 1986; Cati et al., 1987; Ciarapica et al.,
1300 1986; Doglioni & Bosellini, 1987; Jadoul et al., 1992; Shonborn, 1992, 1999; Bertotti et al.,
1301 1993; Zappaterra, 1994; Greber et al., 1997; De Zanche et al., 2000; Franciosi & Vignolo, 2002;
1302 Jadoul et al., 2002; Fantoni & Scotti, 2003; Fantoni et al., 2003, 2004; Berra et al., 2009;

1303 Bertello et al., 2010; Fantoni & Franciosi, 2010; Ponton, 2010; Gianolla et al.,2012, Masetti et
1304 al., 2012; Handy et al., 2014; Pfiffner, 2014.

1305

1306

1307 Fig.9 – Synthetic well logs for the Belvedere 1 well (depth is in metres): (a) Chrono- & Litho-
1308 stratigraphy; (b) Formation pressure model showing the significant increase in overpressure
1309 below 2000m through the Tertiary foredeep clastics and basinal carbonates into the highly
1310 overpressured deep carbonate aquifer consisting of Liassic and Triassic platform limestones
1311 and dolomites; (c) temperature model showing good correspondence between corrected well
1312 temperature measurements and the prediction from the basin model. The average temperature-
1313 depth trend for the Western Po Valley from Pasquale et al (2012) together with the observed
1314 range is also shown; and (d) thermal maturity model showing match of various models to the
1315 dataset from Chiaramonte & Novelli (1986).

1316

1317

1318 Fig.10 - Heat flow histories of the Po Valley and surrounding regions (see text for explanations).

1319

1320 Fig.11 - 1D Transformation Ratio (TR) maturity histories for four wells from the Po Valley
1321 based on initial source rock parameters outlined in Table 1 (TR scale is 0-100): (a) Cerano-1
1322 from the western Po Valley; (b) Belvedere-1 from the central Po Valley; (c) a pseudo-well from
1323 the east-central Po Valley; and (d) Ballan-1 from the eastern Po Valley (see Fig. 2 for well
1324 locations). Vitrinite reflectance maturities are shown as blue lines (note that for wells in (a) and
1325 (b), two histories are shown for the last 10Ma: one based on the geological heat flow and one
1326 based on reduced heat flow from end Miocene times to replicate the effect of overpressure;
1327 wells in (c) and (d) lie outside of the overpressure cell; see text for explanations).

1328

1329 Fig.12 - Transformation ratio (TR) maturity maps (TR scale is 0-1) for the middle Triassic (a-
1330 c) and the Late Triassic (d-f) source intervals, for end Jurassic (a, d), end-Cretaceous (b, e) and
1331 end Miocene (c, f) times. As the onset of overpressure within the carbonate sequences is
1332 interpreted to occur at end Miocene, there is no difference between the maturity levels
1333 associated with the geological heat flow and the overpressure models for this time interval.

1334

1335 Fig.13 – Present day transformation ratio (TR) maturity maps (TR scale is 0-1) for the middle
1336 Triassic (a and b) and the Late Triassic (c and d) source intervals; (a) and (c) show the results

1337 of geological heat flow model with (b) and (d) showing the results for the overpressure model,
1338 based on the application of reduced Plio-Pleistocene heat flow as described in the text.

1339

1340 Fig.14 – Charge timing versus trap formation in the Western Po Valley based on preferred
1341 Overpressure Model (see text for discussion). Vertical orange arrows indicate the presumed
1342 critical moment for each of the traps, i.e., the time at which the trap formed or the seal became
1343 able to retain a hydrocarbon column.

1344

1345 Fig.15 – Model evaluation: (a) cross plot of observed in place volumes for main traps versus
1346 available charge from kitchen area since the critical moment predicted by the models; (b) cross
1347 plot of observed volumes in-place for main traps versus predicted trapped volumes from the
1348 models; (c) cross plot of observed-GOR versus predicted-GOR from the models. Red data
1349 points and regression lines are for the geological heat flow model, blue data points and
1350 regression lines are for the overpressure model. For plot (b) regression lines have been fitted to
1351 the dataset excluding the Gaggiano outlier. In all plots the black line corresponds to a perfect
1352 match between observation and model.

1353

1354 Table 1 – Po Valley 3D basin modelling workflow and associated working phases.

1355

1356 Table 2 - Table of source rock parameters used in thermal modelling of the Po Valley.
1357 Parameters are from published data on the Po Valley Triassic source intervals as reported for
1358 the Villafortuna-Treccate and Malossa fields, as well as outcrop analogues. Colours correspond
1359 to Gross depositional environments in Fig.8. Kerogen Types A (“Aquatic, marine, siliceous or
1360 carbonate/ evaporitic”) & F (“Terrigenous, non-marine, wax-poor”) are as defined by Pepper
1361 & Corvi (1995 a, b). These are analogous to Kerogen Type IIS and Kerogen Type III/Type IV,
1362 respectively, as by Tissot & Welte (1984).

1363

1364

1365 Table 3 - Table of rock properties used in basin modelling of the Po Valley. Where available,
1366 local rock properties are used (Berra & Carminati, 2010; Pasquale et al, 2011; Pasquale et al,
1367 2012). Other values are from global averages (Gretner, 1981; Waples & Waples, 2004;
1368 Middleton, 1993).

Phase 1 – 1D model building

- Reference well and pseudo-well chrono-litho-stratigraphy, back-stripping parameters, thermal parameters, source rock parameters, temperature and maturity data loaded into Genesis (<http://www.zetaware.com/>);
- Definition of geological heat flow and overpressure models, primarily based on the available literature;
- Collation of information about palaeo-water depth and palaeo-sediment/water interface temperature.

Phase 2 – 1D model calibration and outputs

- Calibration of rock property and present-day heat flow model against temperature data;
- Calibration of back-stripping and heat flow models by forward modelling of thermal maturity and comparison against available maturity data;
- 1D modelling of hydrocarbon generation from key source intervals.

Phase 3 – 3D model building & simulation

- 3D stratigraphic grids exported from the Kingdom package into the Trinity software, with additional grids generated by interpolating between imported grids as necessary, particularly to define source rock intervals;
- Further definition of source intervals within the model, including lateral distribution from gross depositional environment (GDE) maps, thickness and kerogen type as described in the literature;
- Definition of 3D palaeo-temperature model by calibration against 1D models for key wells and pseudo-wells;
- 3D hydrocarbon maturation/generation/migration history modelling across the Po Valley and analysis of kitchen areas associated with key traps.

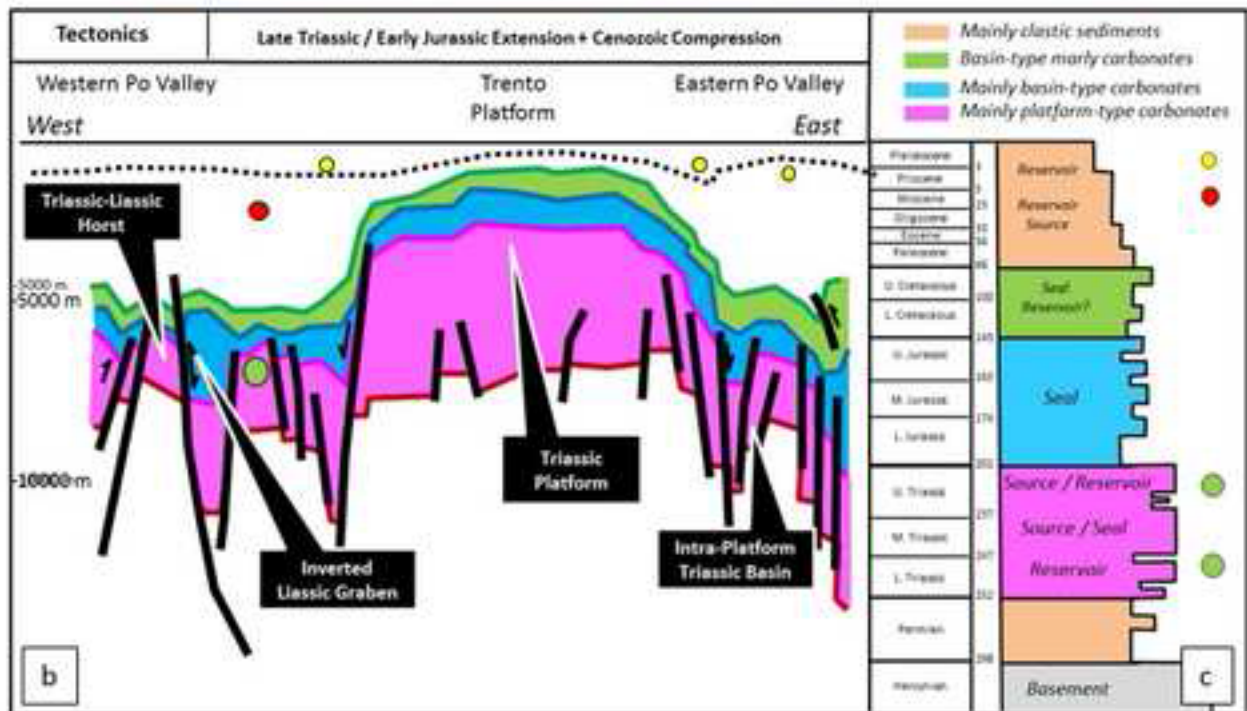
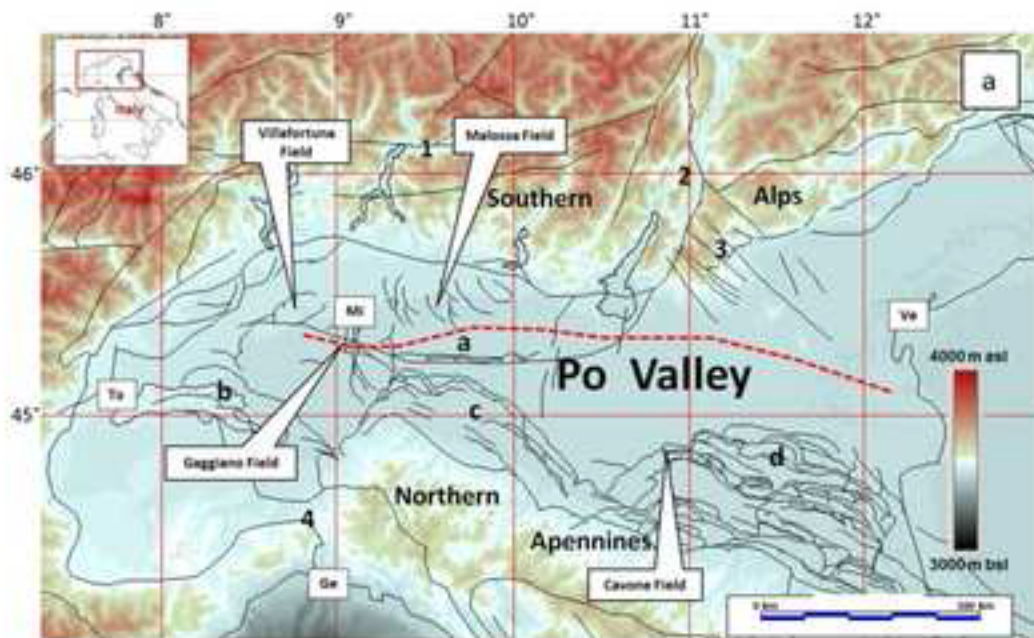
Table 2 – Source rock parameters

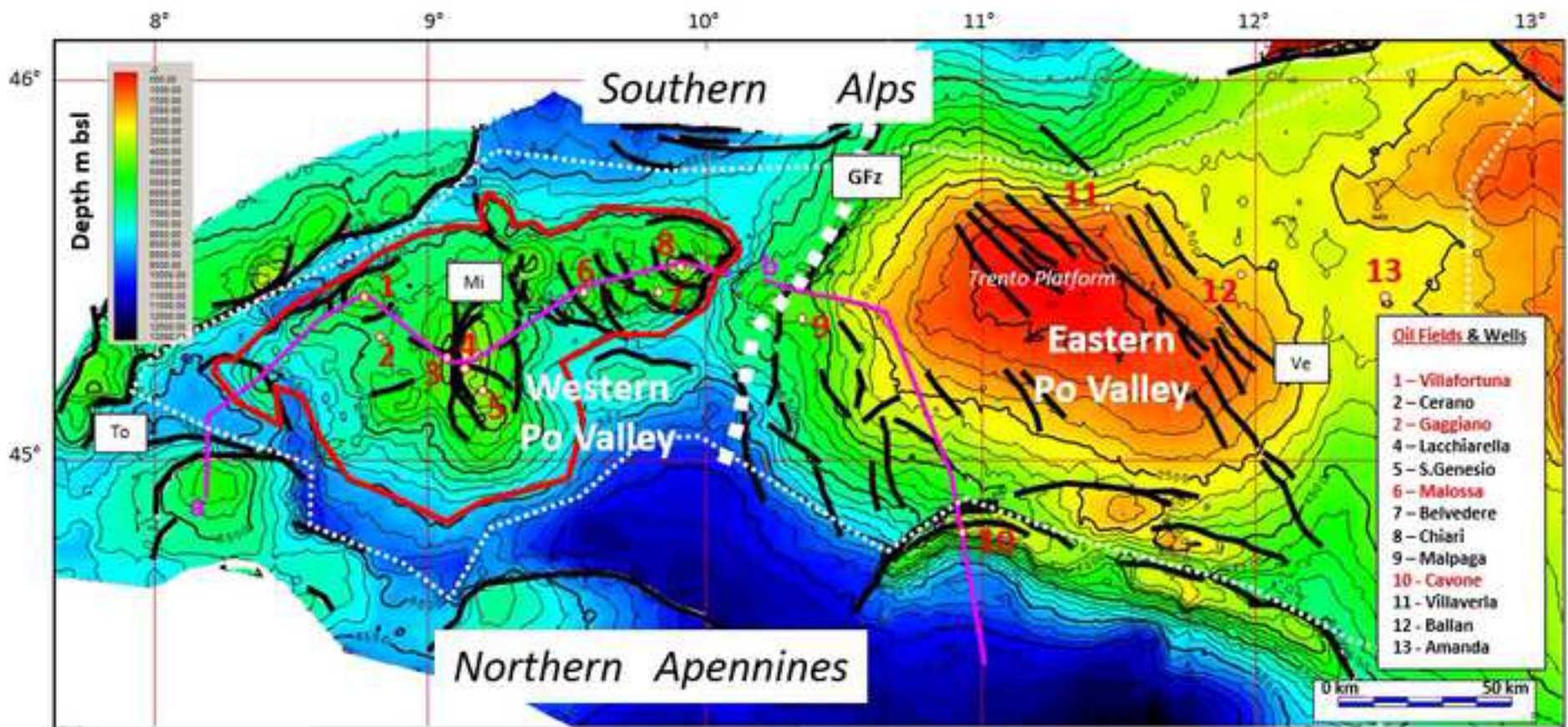
| Source Age Interval | Domain | Formation(s) | Net Thickness (m) | TOC (%) | Kerogen Type | | Weight (%) | Hydrogen Index | Petroleum Potential | | |
|---------------------|----------------------------|--|-------------------|---------|----------------------|-----------------------|------------|----------------|---------------------|------------------------|---------------------|
| | | | | | Tissot & Welte, 1984 | Pepper & Corvi, 1995a | | | mg HC/ g Rock | mmbbl/ Km ² | bct/Km ² |
| Upper Triassic | Long-lived anoxic basin | Argille di Riva di Solto, Formi | 50 | 4 | II S | A | 90 | 550 | 19.8 | 17.9 | |
| | | | | | III | F | 10 | 160 | 0.64 | | 3.9 |
| | Intra-platform/ramp lagoon | Dolomia Principale, Monticello, Calcare di Zu, Scisti Bituminosi | 12.5 | 4 | II S | A | 90 | 550 | 19.8 | 4.5 | |
| | | | | | III | F | 10 | 160 | 0.64 | | 1 |
| Middle Triassic | Long-lived anoxic basin | Meride, Besano | 50 | 4 | II S | A | 90 | 550 | 19.8 | 17.9 | |
| | | | | | III | F | 10 | 160 | 0.64 | | 3.9 |
| | Episodically anoxic basin | Meride, Livinallongo, Moena, Rio del Lago | 25 | 4 | II S | A | 90 | 550 | 19.8 | 9 | |
| | | | | | III | F | 10 | 160 | 0.64 | | 2 |
| | Intra-platform/ramp lagoon | Gorno | 12.5 | 4 | II S | A | 10 | 550 | 2.2 | 4 | |
| | | | | | III | F | 90 | 160 | 5.76 | | 70.9 |

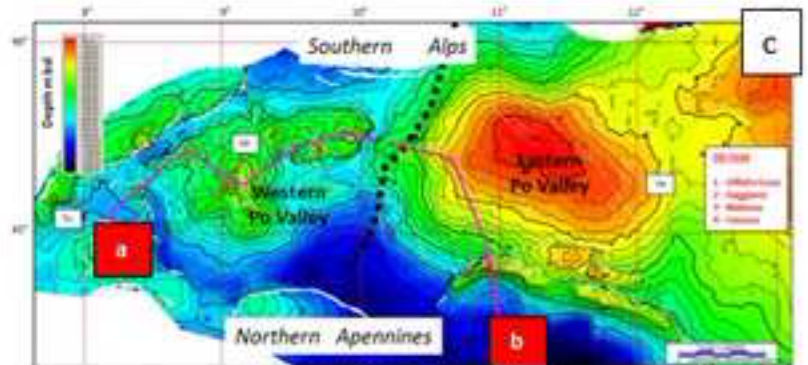
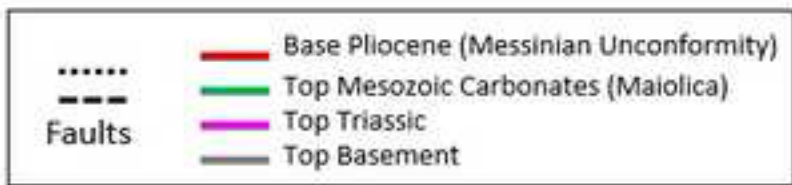
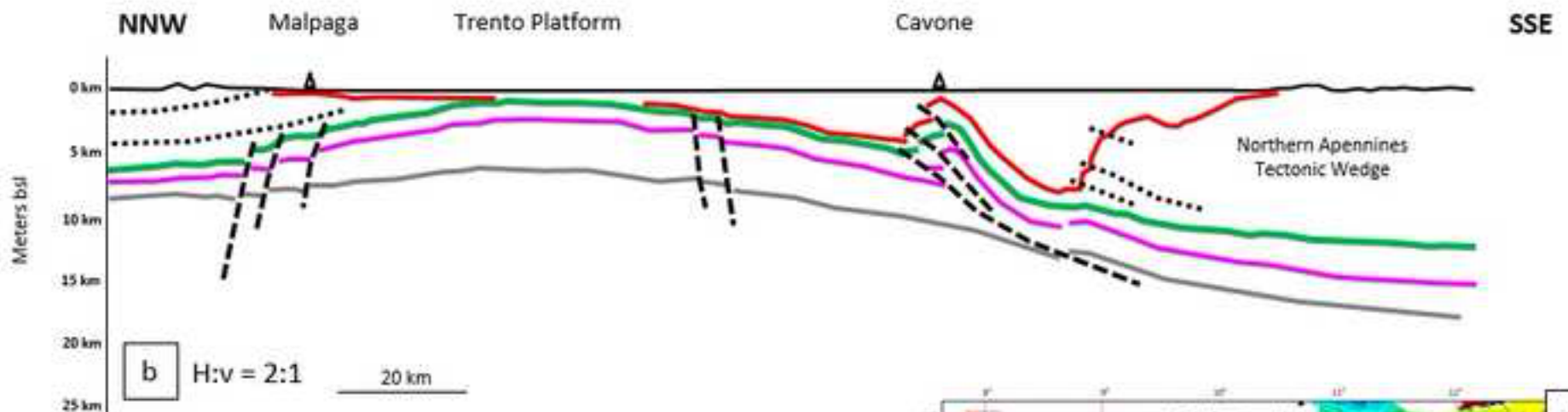
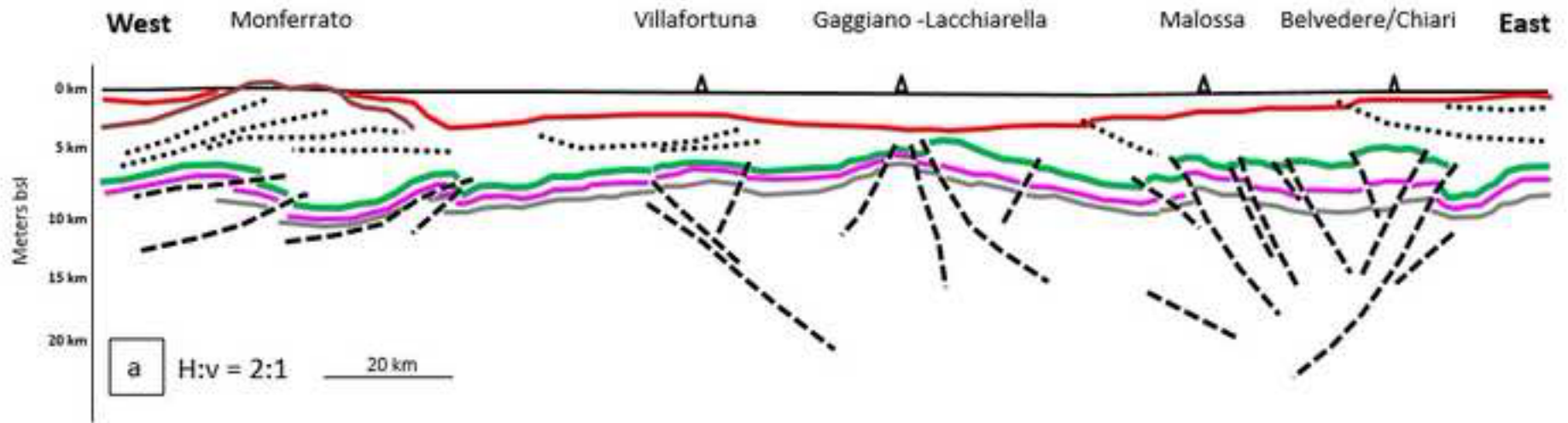
Table 3 – Rock properties

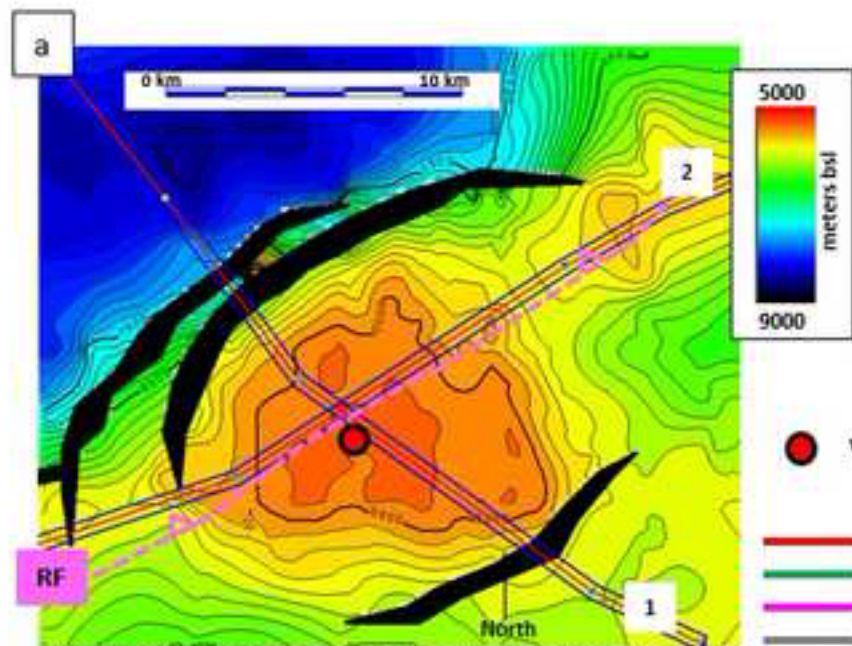
| Rock Properties | | | | | | | | | | |
|--|---------|-----------|--------|------------------------|-----------|----------|-----------|--------|--------|--------------|
| Rock Type | Shale | Sandstone | Chalk | Chert/ Radiolarites | Limestone | Dolomite | Anhydrite | Silt | Marl | Conglomerate |
| Surface porosity | 0.29 | 0.28 | 0.70 | 0.70 | 0.51 | 0.30 | 0.63 | 0.29 | 0.50 | 0.40 |
| Compaction Coefficient | 0.38 | 0.22 | 0.71 | 0.71 | 0.52 | 0.22 | 0.52 | 0.38 | 0.54 | 0.23 |
| Porosity at 3000m (using Athy eq. $\phi(z) = \phi_0 e^{-\alpha z}$) | 0.09 | 0.15 | 0.08 | 0.08 | 0.11 | 0.16 | 0.13 | 0.09 | 0.10 | 0.20 |
| Bulk density (kg/m ³) | 2720 | 2650 | 2710 | 2650 | 2710 | 2710 | 2270 | 2650 | 2715 | 2650 |
| Thermal conductivity (w/m/K) | 1.62 | 3.85 | 3.14 | 7.11 | 3.14 | 4.98 | 4.76 | 3.35 | 2.25 | 4.18 |
| Temperature Dependency of thermal conductivity (1/C) | -0.0004 | 0.0019 | 0.0015 | 0.0030 | 0.0015 | 0.0025 | 0.0024 | 0.0016 | 0.0010 | 0.0021 |
| Specific heat (J/kg/°K) | 832 | 735 | 815 | 740 | 815 | 870 | 585 | 784 | 824 | 812 |
| Specific heat (cal/g/°C) | 0.20 | 0.18 | 0.19 | 0.18 | 0.19 | 0.21 | 0.14 | 0.19 | 0.20 | 0.19 |
| Radiogenic heat (μW/m ²) | 1.33 | 1.05 | 0.63 | 0.43 | 0.45 | 0.46 | 0.09 | 1.13 | 0.92 | 0.90 |

| | | |
|-----------------|-------------------------|----------------------|
| Gretner, 1981 | Waples & Waples, 2004 | Pasquale et al, 2011 |
| Middleton, 1993 | Berra & Carminati, 2010 | Pasquale et al 2012 |
| | Sekiguchi, 1984 | |









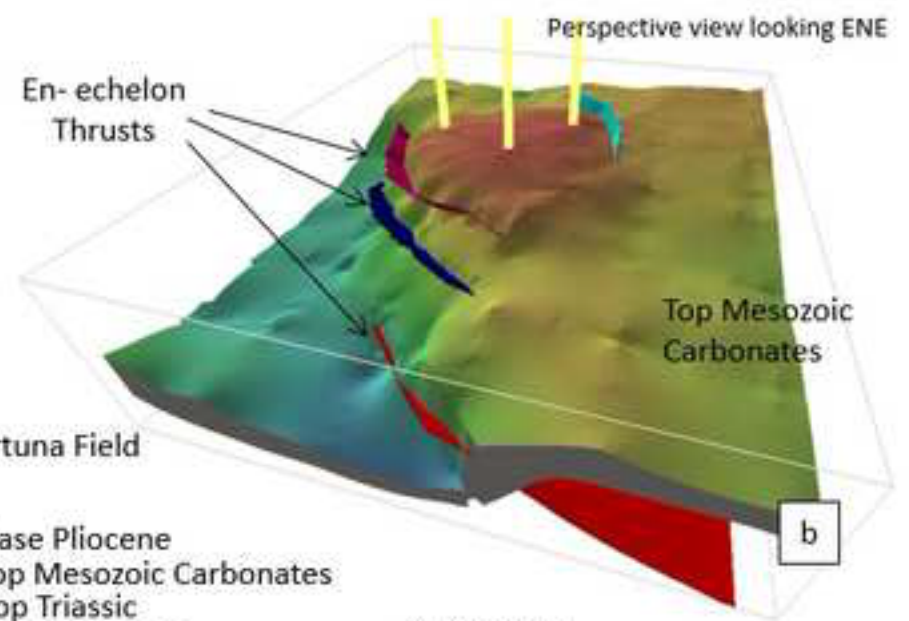
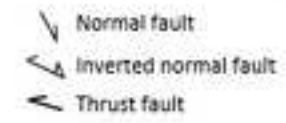
Top Mesozoic Carbonates Depth map (contour interval is 100 m)

● Villafortuna Field



Base Pliocene
Top Mesozoic Carbonates
Top Triassic
Top Basement

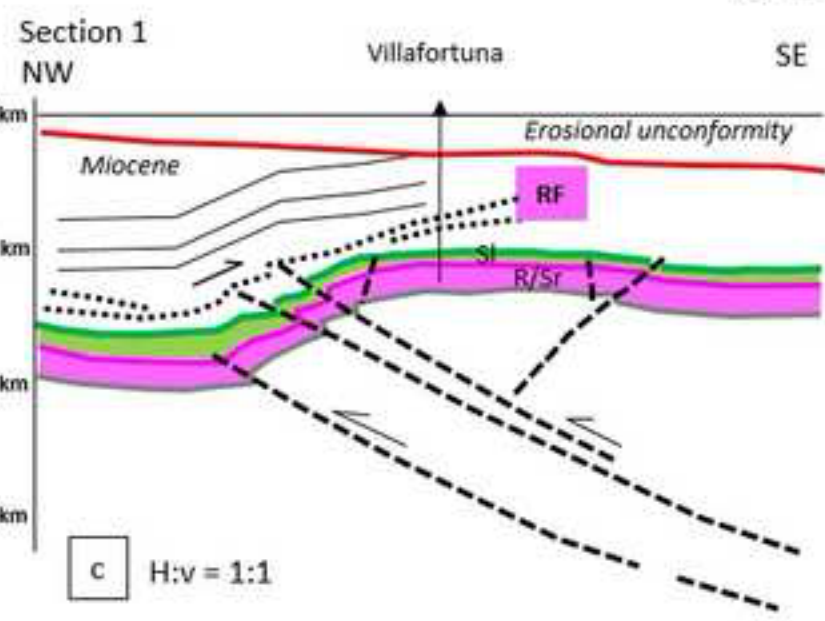
Faults



Perspective view looking ENE

En-echelon Thrusts

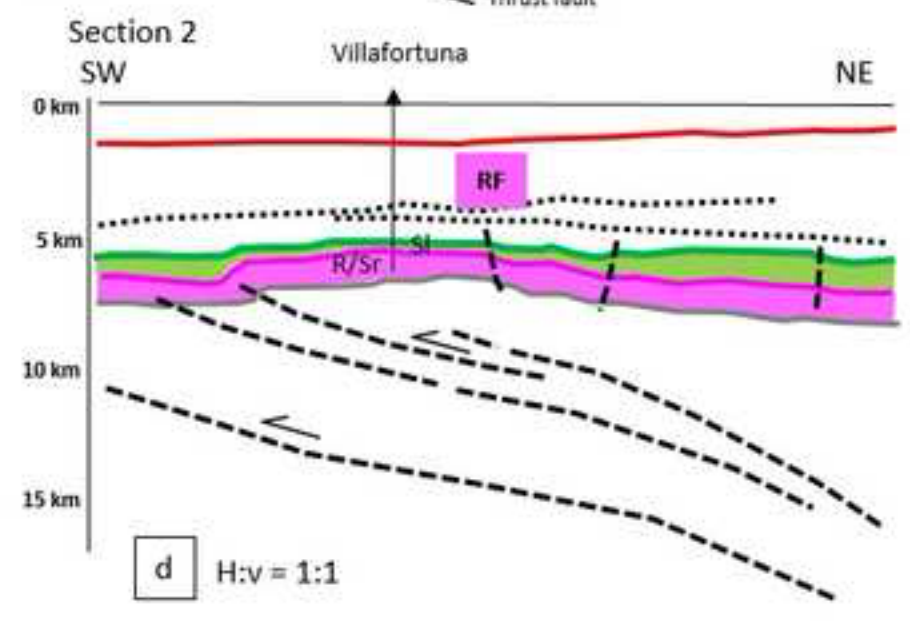
Top Mesozoic Carbonates



Section 1
NW SE

Villafortuna

c H:v = 1:1

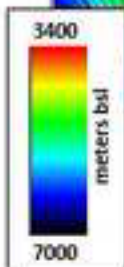
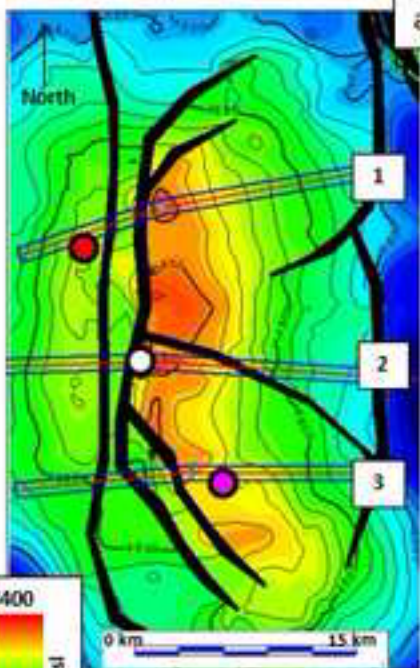


Section 2
SW NE

Villafortuna

d H:v = 1:1

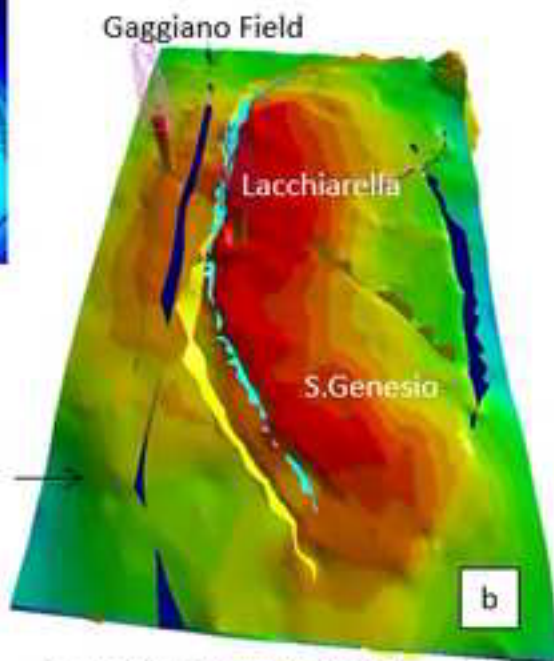
Top Mesozoic Carbonates Depth map
(contour interval is 200 m)



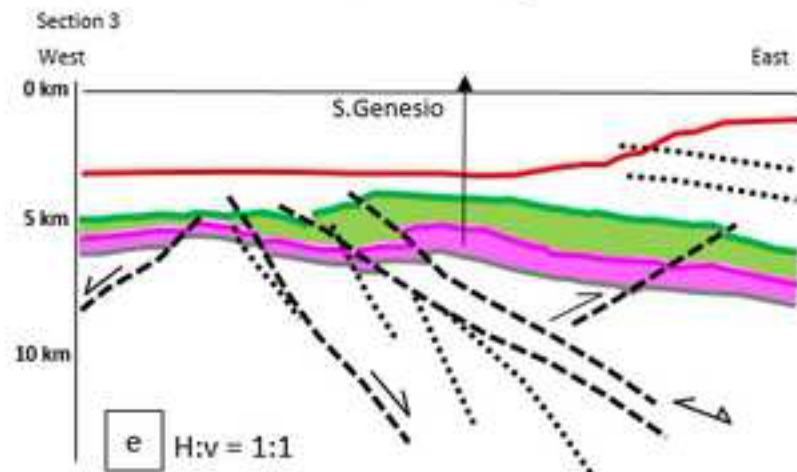
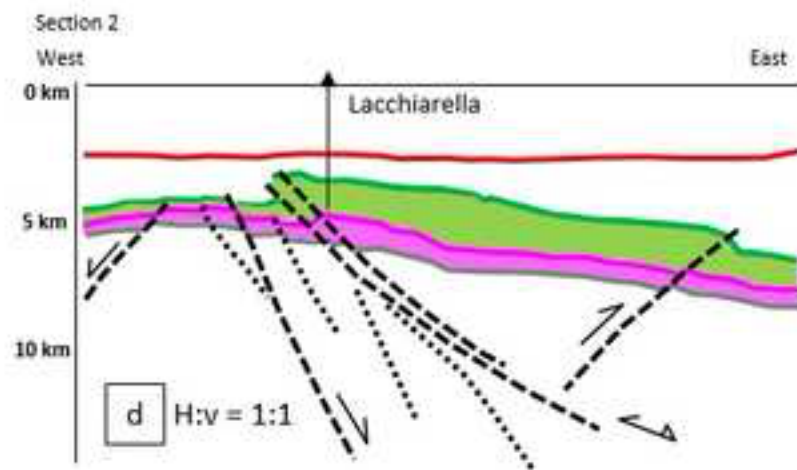
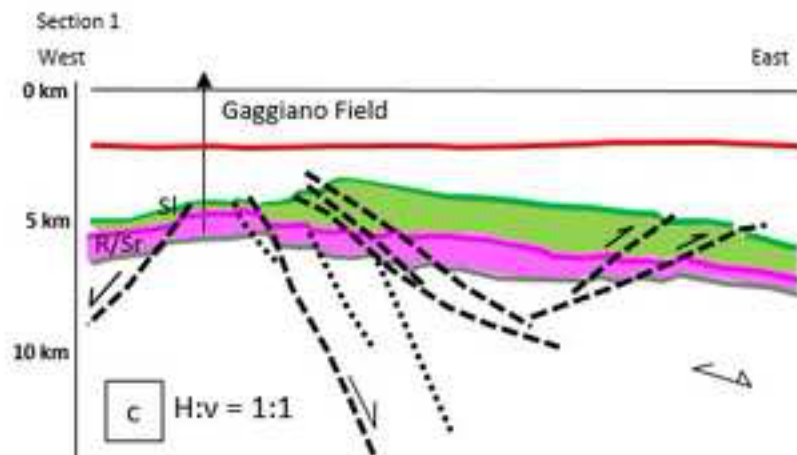
- Normal fault
- Inverted normal fault
- Thrust fault

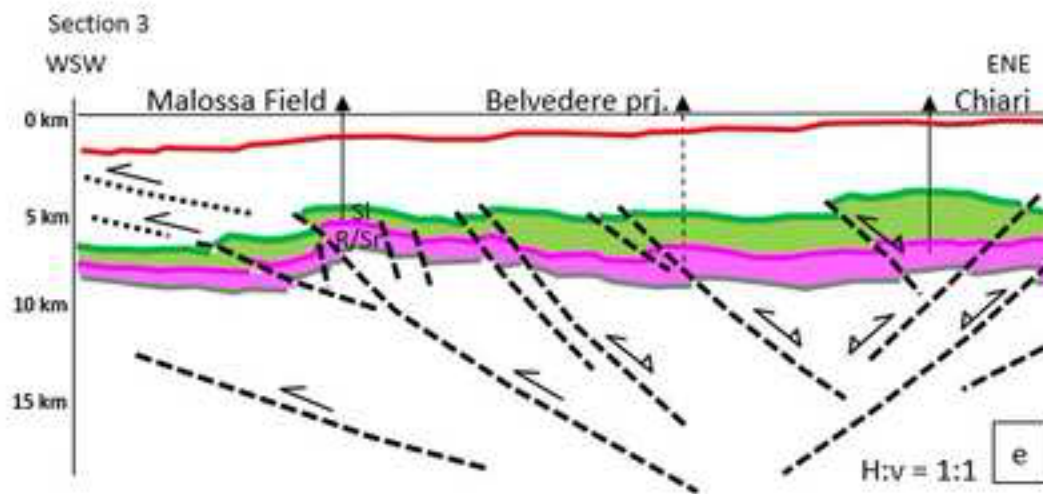
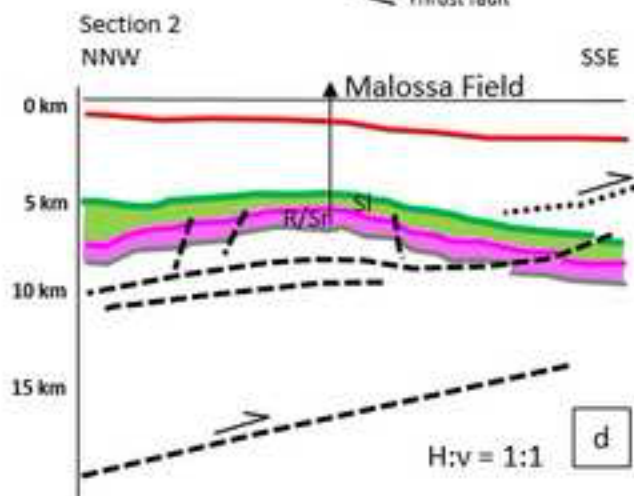
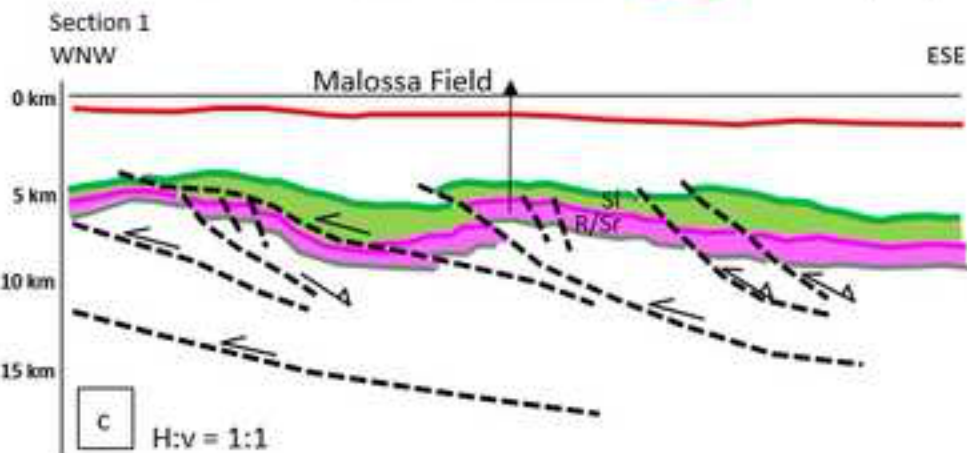
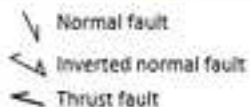
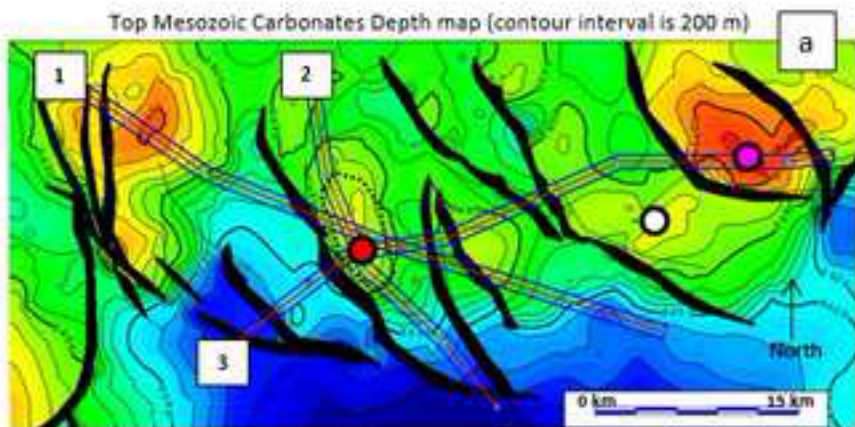
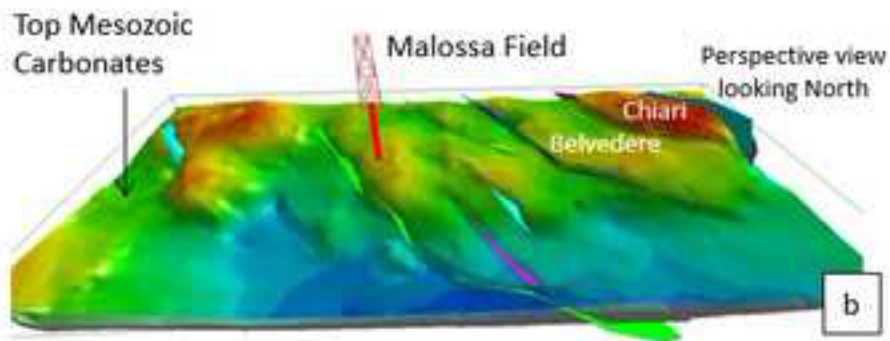
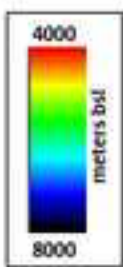
- Top Mesozoic Carbonates
- Top Triassic
- Top Basement
- Faults
- Gaggiano Field
- Lacchiarella
- S.Genesio

Top Mesozoic Carbonates

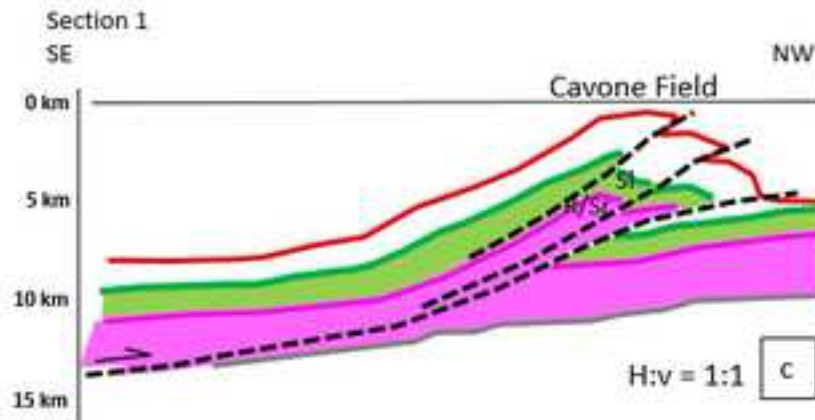
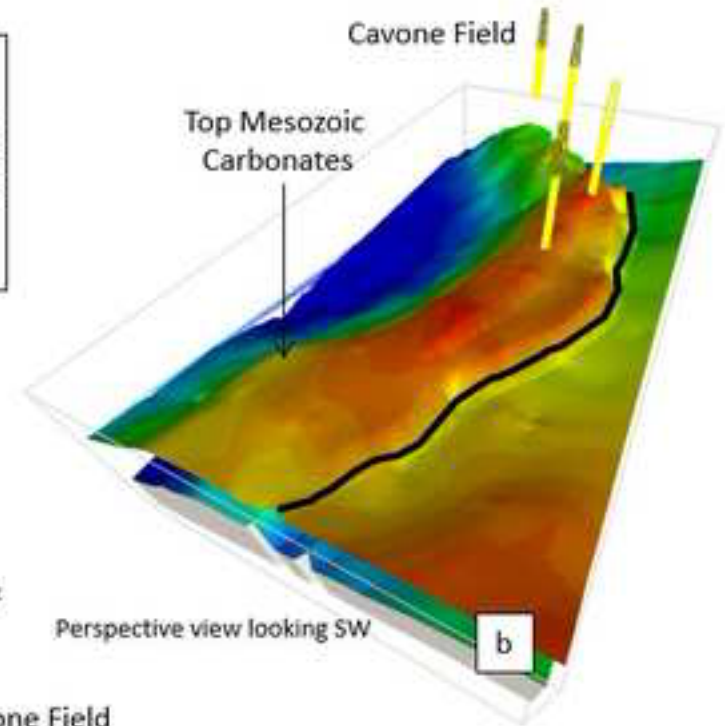
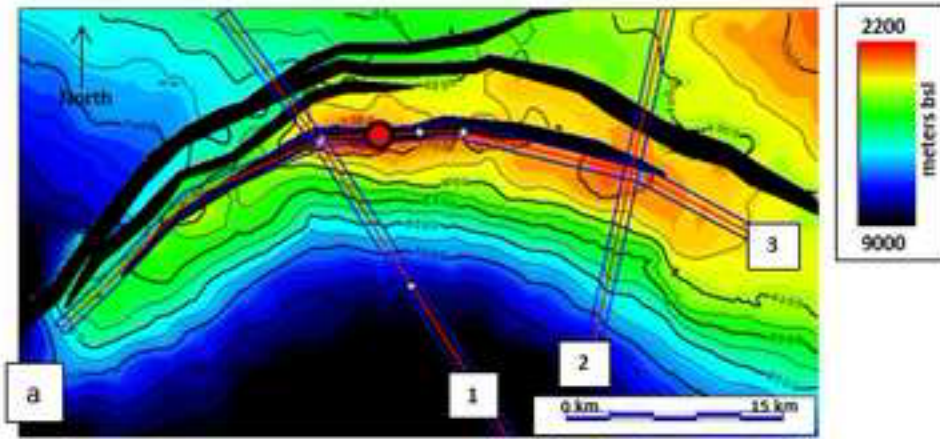


Perspective view looking North



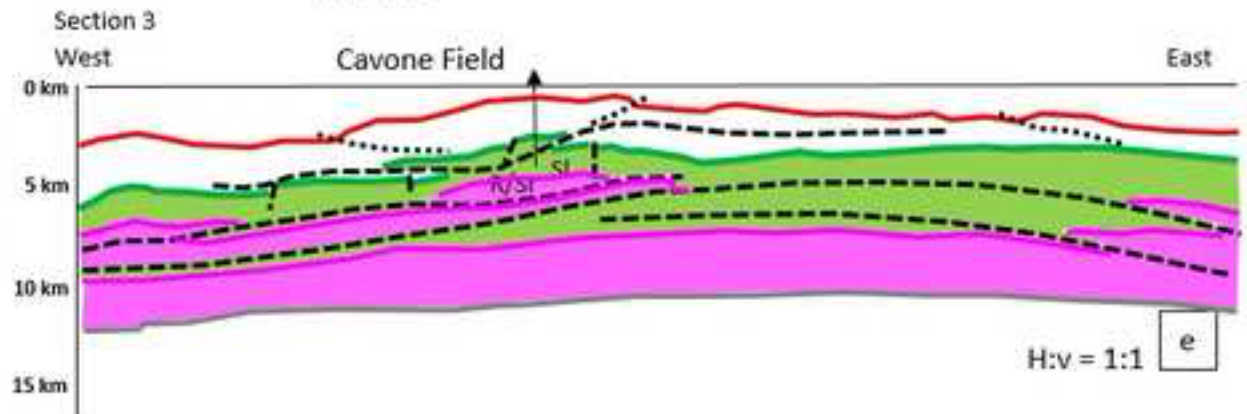
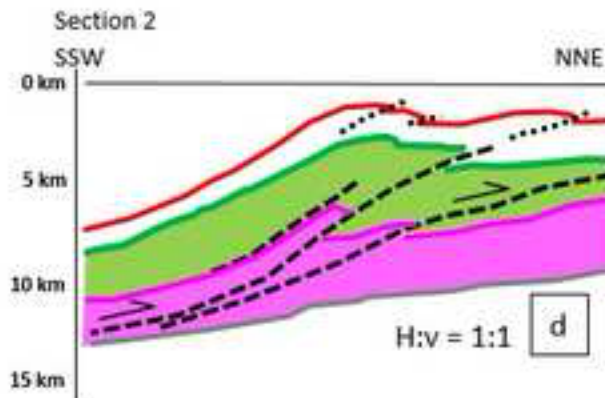


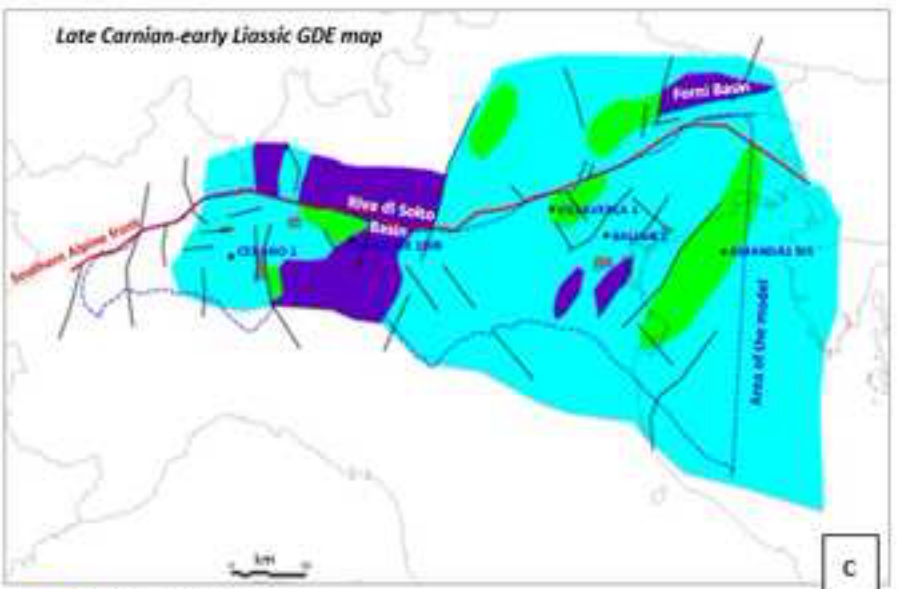
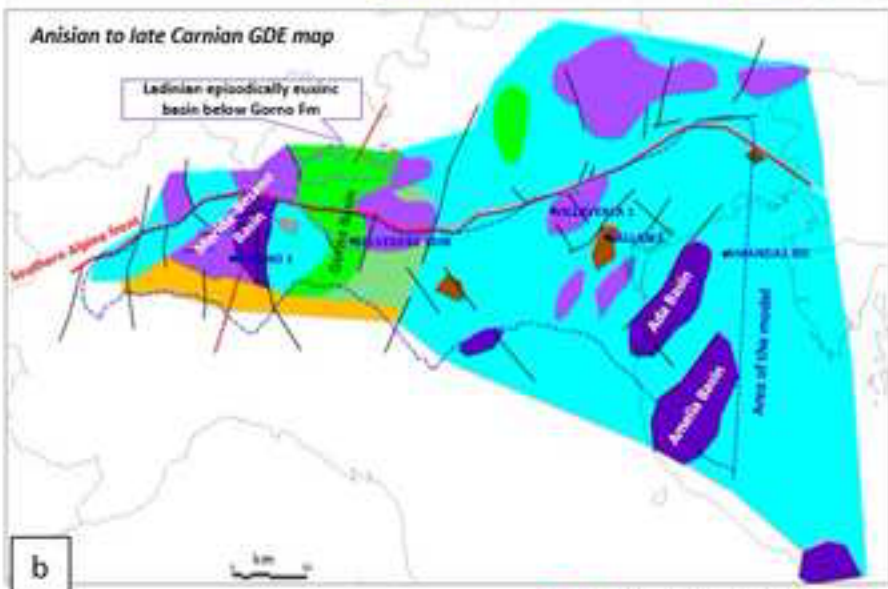
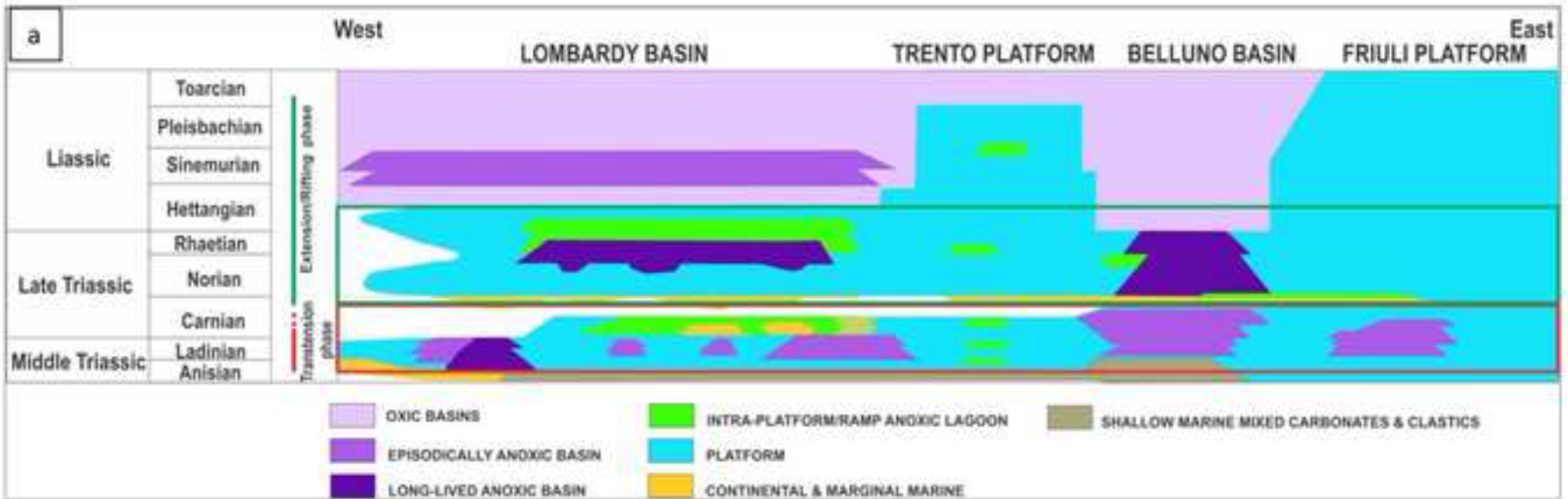
Top Mesozoic Carbonates Depth map (contour interval is 500 m)



- ↘ Normal fault
- ↗ Inverted normal fault
- ↖ Thrust fault

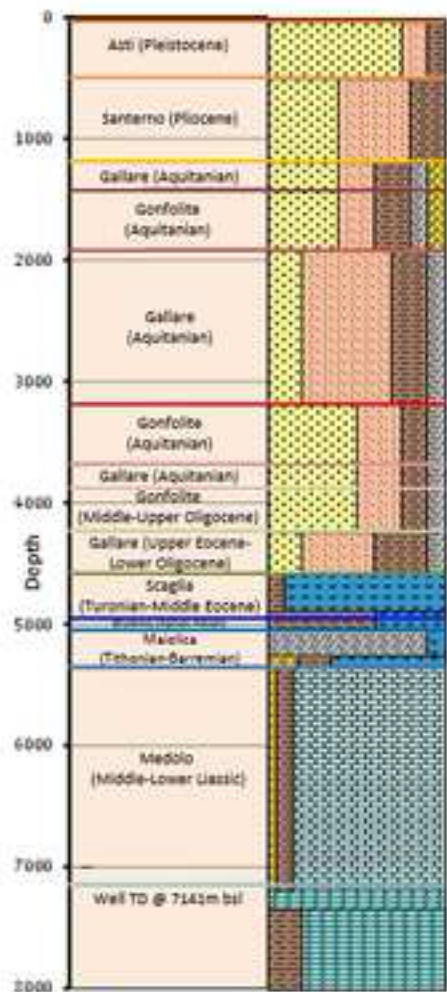
- Cavone Field
- Base Pliocene
- Top Mesozoic Carbonates
- Top Triassic
- Top Basement
- ⋯ Faults



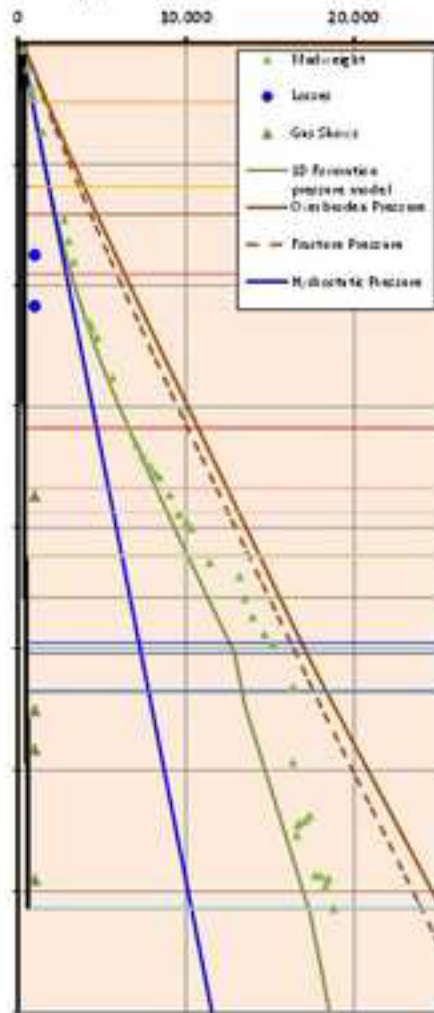


- | | |
|-----------------------------------|---------------------------------------|
| Shallow water carbonates | Delta Continental |
| Long-lived anoxic basin | Platform passing to delta/continental |
| Episodically anoxic basin | Igneous |
| Intra-platform/ramp anoxic lagoon | Emerged areas |

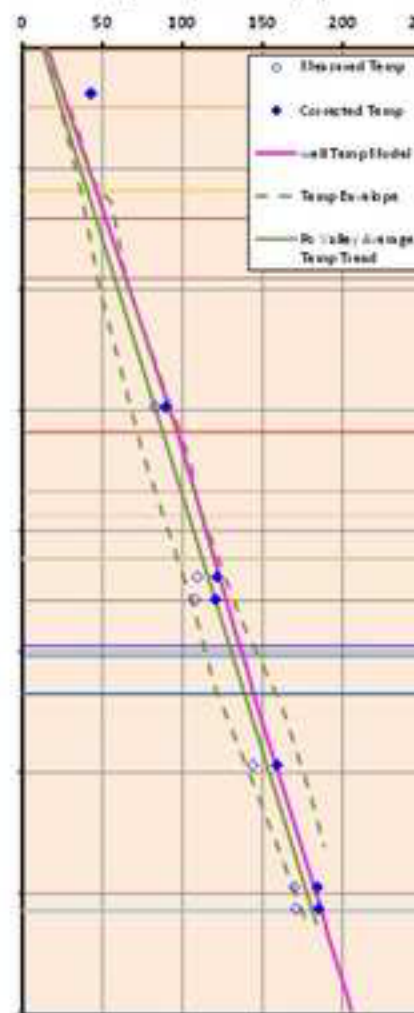
(a) Litho-stratigraphy



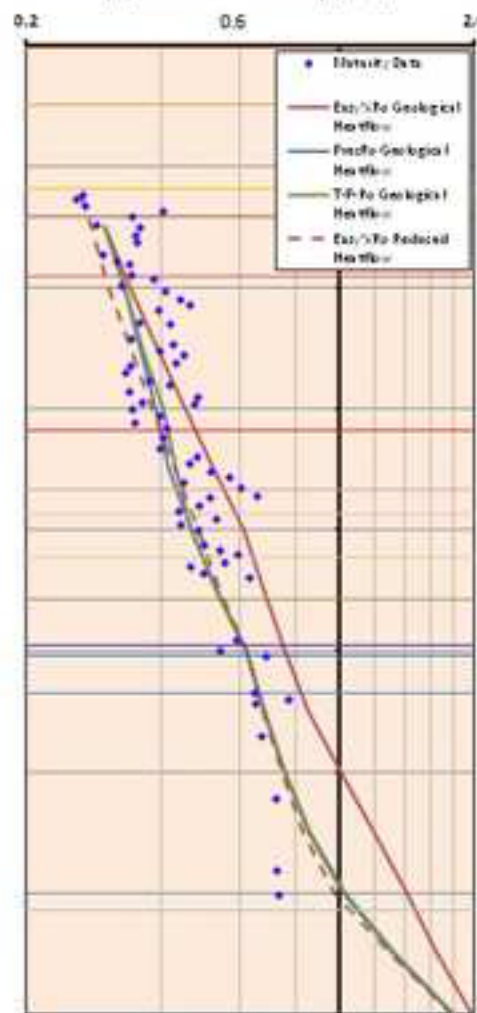
(b) Formation Pressure (psi)

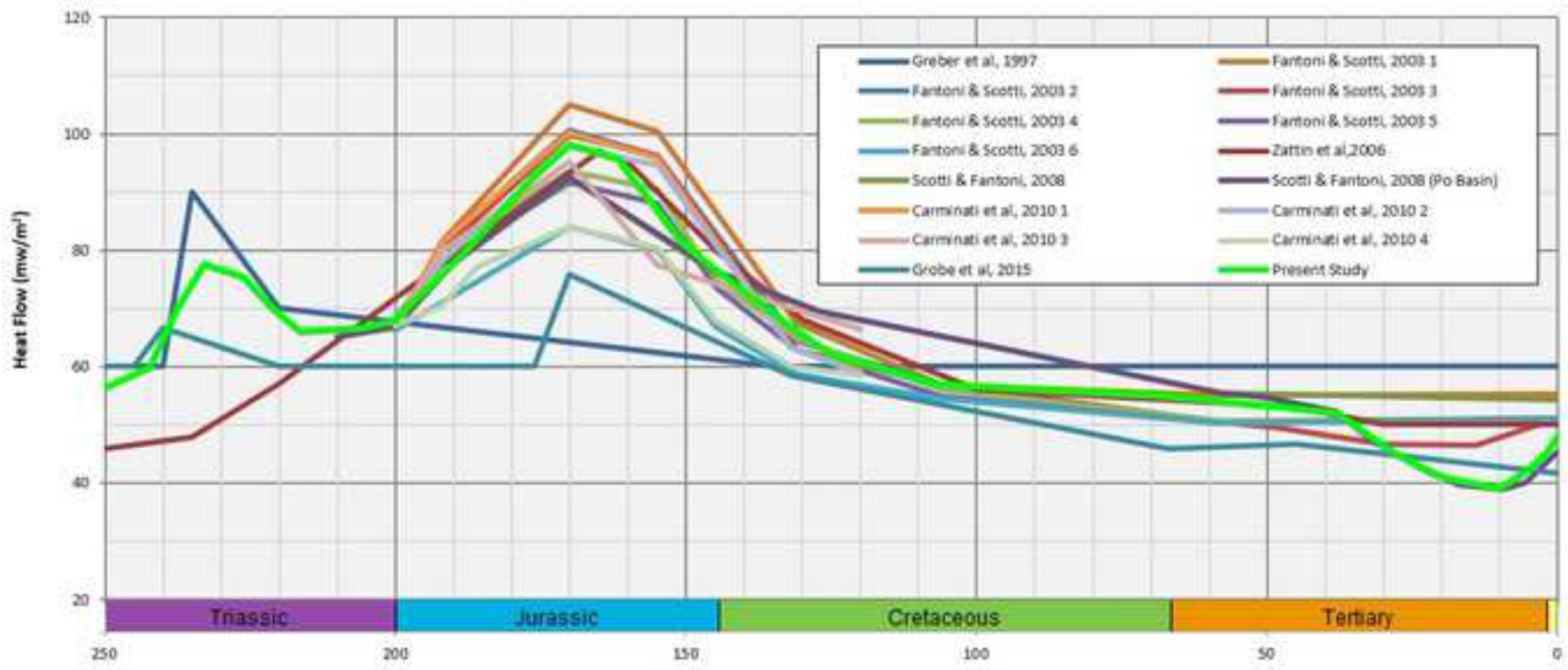


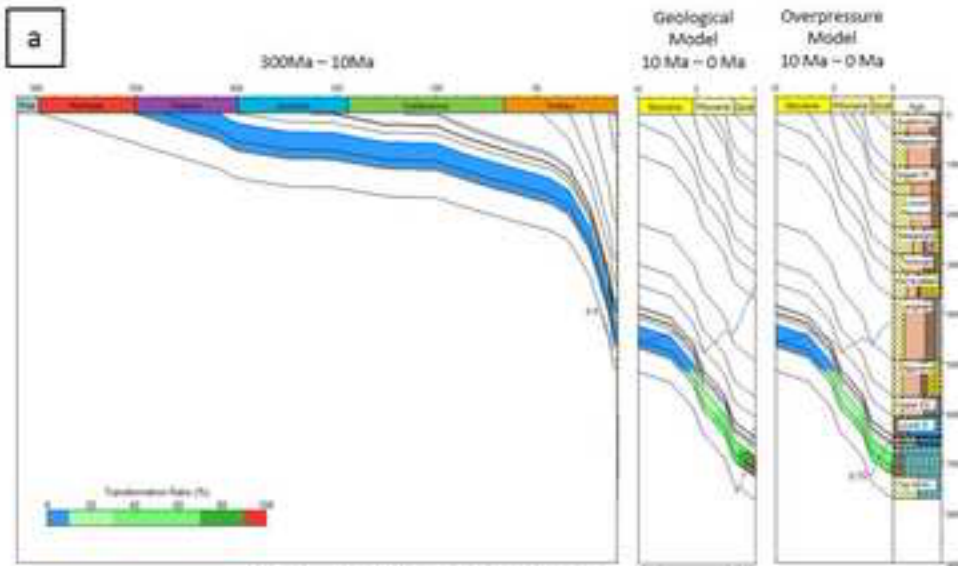
(c) Temperature (°C)



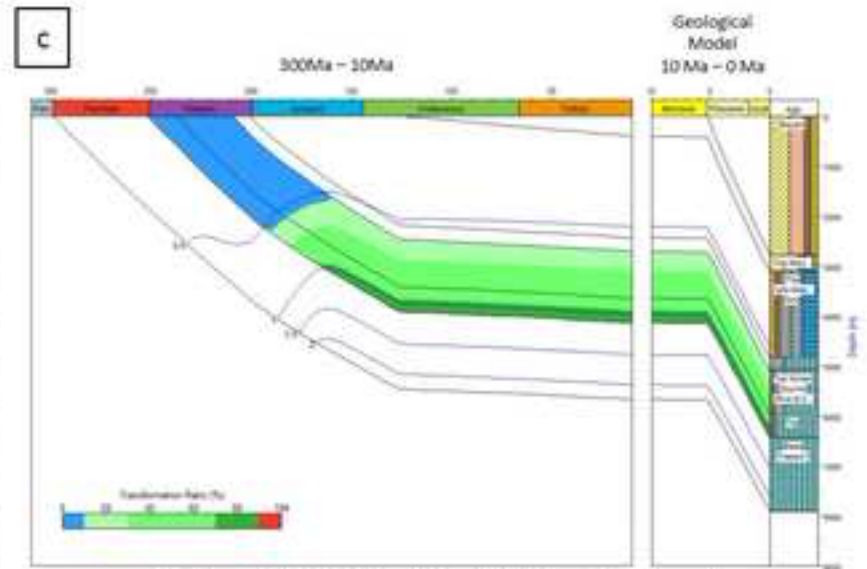
(d) Thermal Maturity (%R_o)



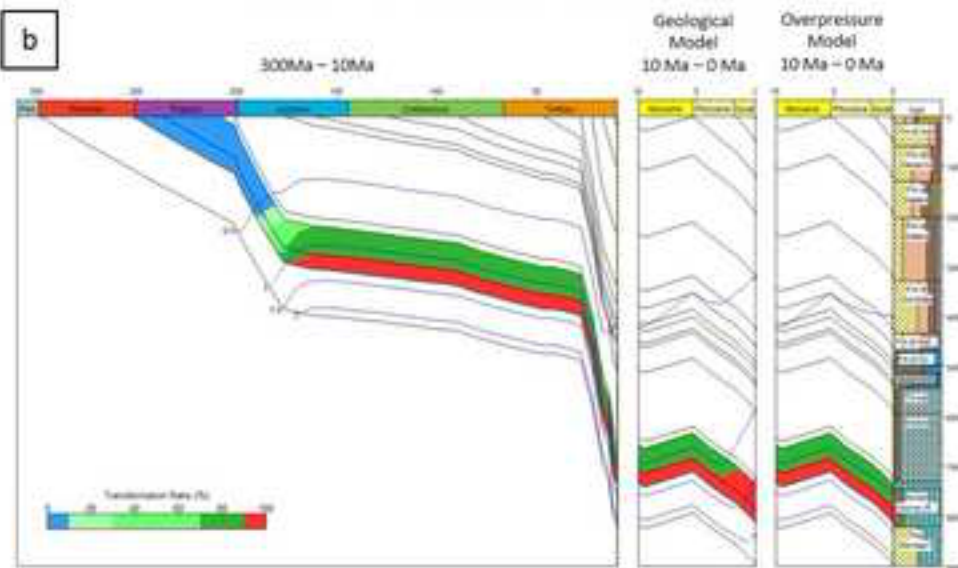




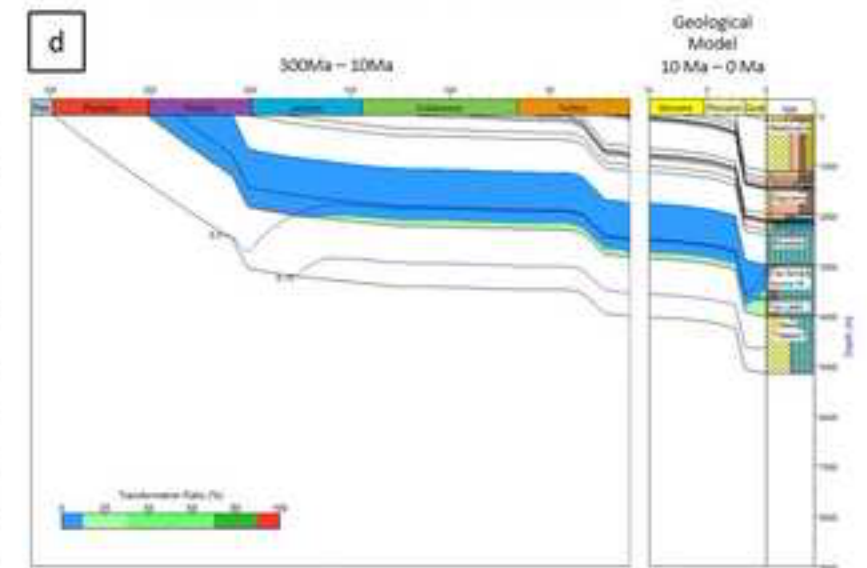
Western Po Valley Maturity History (Cerano-1)



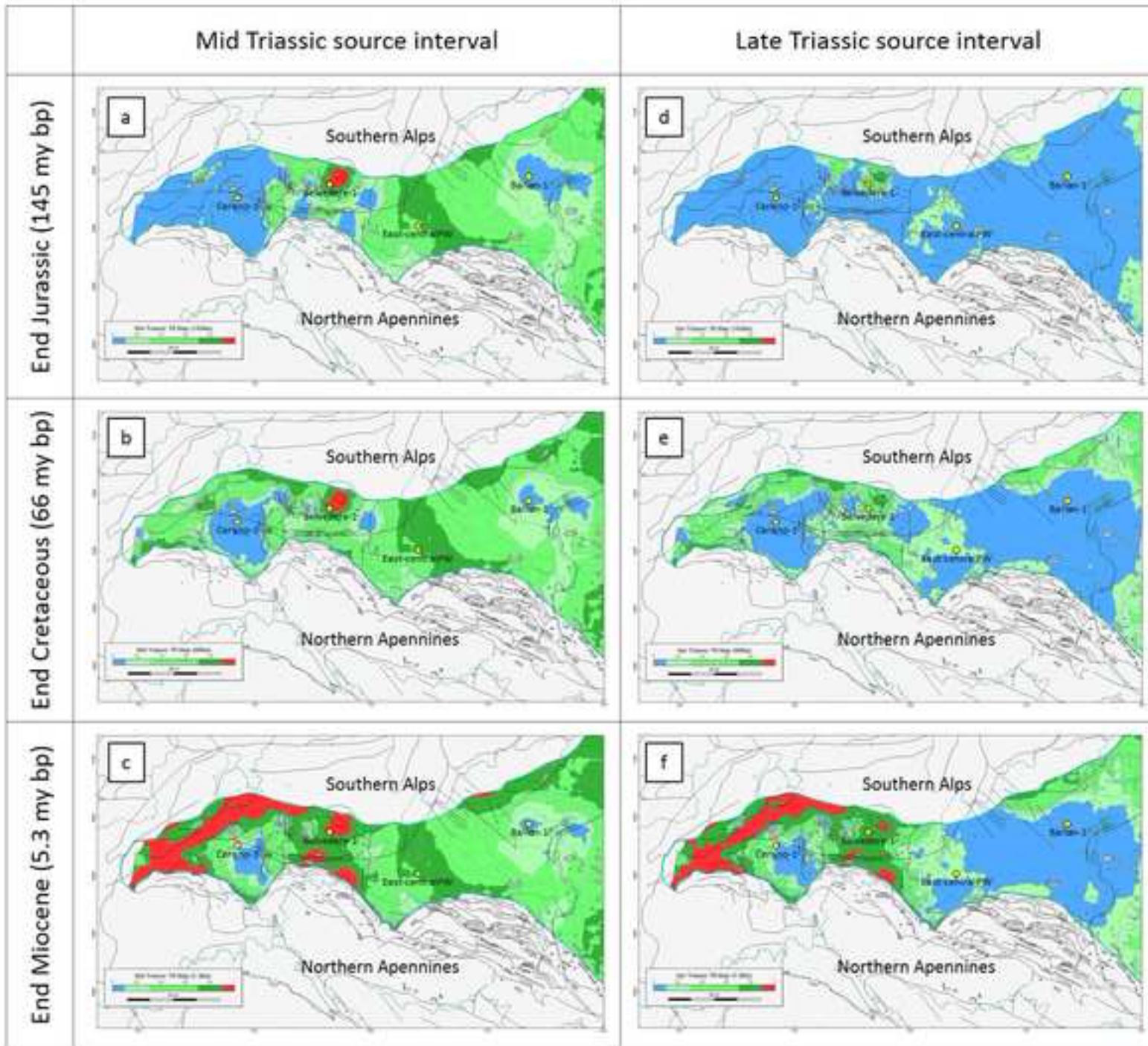
East-central Po Valley Maturity History (Pseudowell)



Central Po Valley Maturity History (Belvedere-1)



Eastern Po Valley Maturity History (Ballan-1)



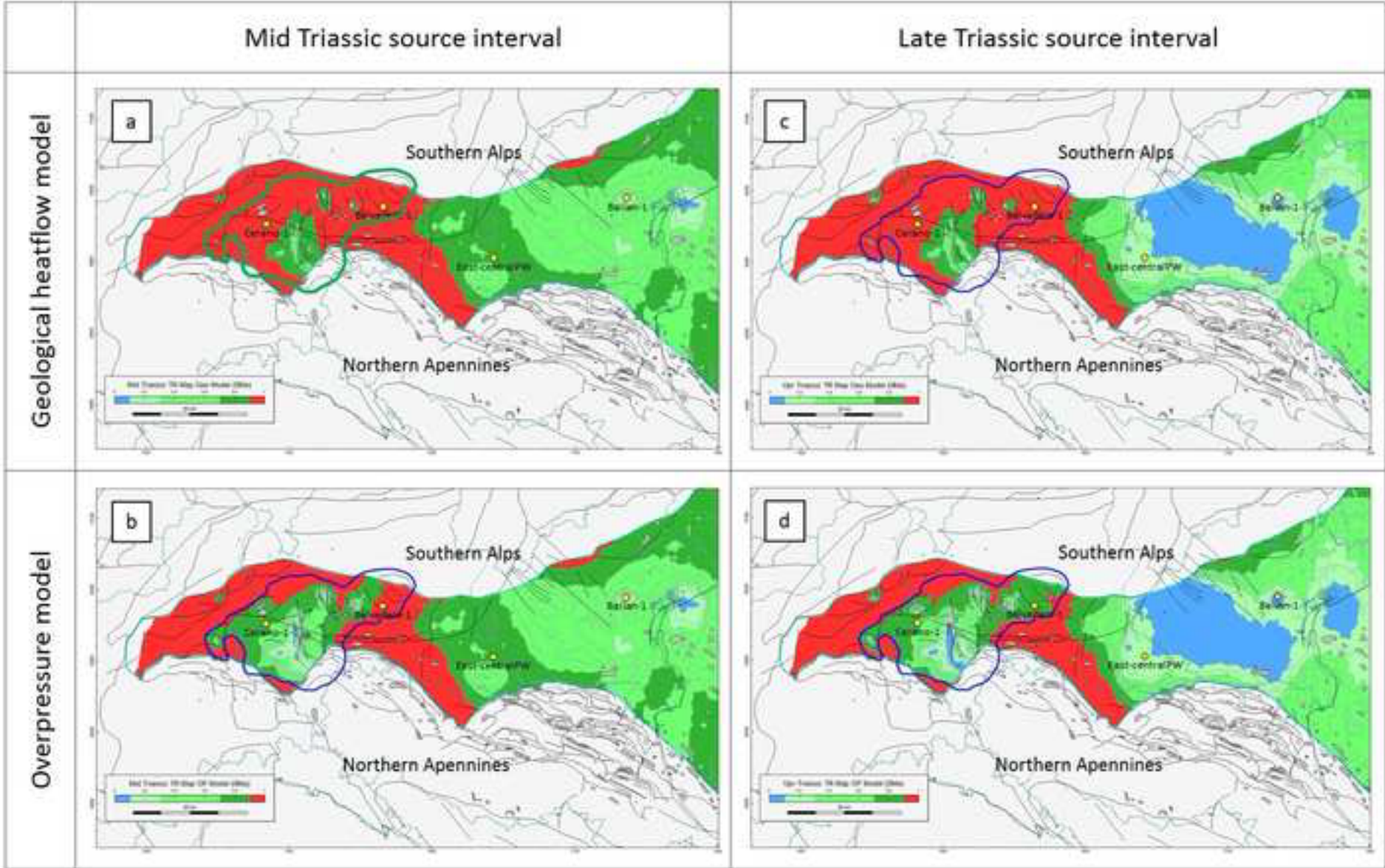


Fig.14

